Electronic Supplementary Information

3D Nitrogen-Doped Carbon Frameworks with Pore Hierarchy and Graphitic Carbon Channels for High-Performance Hybrid Energy Storages

Jae Won Choi[a,b], Dong Gyu Park[a], Keon-Han Kim[c], Won Ho Choi[d], Min Gyu Park[a,e] and Jeung Ku Kang[*a]

[a.] *Department of Materials Science and Engineering, NanoCentury Institute, Korea Advanced Institute of Science and Technology (KAIST), 291 Daehak-ro, Yuseong-gu, Daejeon 34141, Republic of Korea*

[b.] *Materials Architecturing Research Center, Korea Institute of Science and Technology (KIST), 14-gil 5 Hwarang-ro, Seongbuk-gu, Seoul 02792, Republic of Korea*

[c.] *Chemical Science Division, Lawrence Berkeley National Laboratory, 1 Cyclotron Road, Berkeley, CA 94720, USA*

[d.] *Department of Petrochemical Materials, Chonnam National University, 50 Daehak-ro, Yeosu-si 59631, Republic of Korea*

[e.] *Advanced Cell Platform Group, Samsung SDI, 150-20 Gongse-ro, Giheung-gu, Yongin-Si, Gyeonggi-do, 17084, Republic of Korea*

[*] *Email: jeungku@kaist.ac.kr*

Section S1. Experimental Procedures

Synthesis of Co_x-Zn_{10-x} metal-organic framework/graphene oxide (MOF/GO) structures

Graphene oxide (GO) was prepared from graphite flake (Alfa Aesar) using the improved Hummers method as reported in the literature.[1] First, 20 mg of GO is dispersed in 40 ml deionized (DI) water, and 23.28 mg (0.08 mmol) of $Co(NO_3)_2 \cdot 6H_2O$ and 214.19 mg (0.72 mmol) of $Zn(NO_3)_2 \cdot 6H_2O$ were dispersed in 40 ml DI water. They were mixed and stirred at room temperature. Then, 1.313 g (16 mmol) of 2-methylimidzole in 80 ml of DI water was added and vigorously stirred at room temperature for 24 h. The resulting suspension was centrifuged to collect precipitants, then washed with DI water three times and freeze-dried for 3 days. The other Co_x-Zn_{10-x} MOF/GO samples were also synthesized in the same way besides the proportion of $Co(NO_3)_2 \cdot 6H_2O$ with $Zn(NO_3)_2 \cdot 6H_2O$. Their total amount was fixed to 0.8 mmol, such as Zn-MOF/GO (0.8 mmol of $Zn(NO_3)_2 \cdot 6H_2O$), Co_2-Zn_8 MOF/GO (0.16 mmol of $Co(NO_3)_2 \cdot 6H_2O$, 0.64 mmol of $Zn(NO_3)_2 \cdot 6H_2O$), Co_3-Zn_7 MOF/GO (0.24 mmol of $Co(NO_3)_2 \cdot 6H_2O$, 0.56 mmol of $Zn(NO_3)_2 \cdot 6H_2O$) and Co-MOF/GO (0.8 mmol of $Co(NO_3)_2 \cdot 6H_2O$).

Synthesis of Co_x-Zn_{10-x} nitrogen-doped hierarchical porous graphitic carbon (NHPGC) cathode

The freeze-dried Co_x-Zn_{10-x} MOF/GO powder was placed in an alumina boat and then transferred into the quartz tube in rapid thermal chemical vapor deposition (RTCVD) system with Kantal type heater (Tera leader), then heated at 900 °C for 12 h under 200 sccm of Ar flow with a heating rate of 5 °C min^{-1}. After naturally cooling to room temperature, the obtained black powder was dispersed in 1M nitric acid by ultrasonication for 30 min, heated at 80 °C for 2 days, filtered and dried in a vacuum oven.

Synthesis of tin oxides-incorporated NHPGC (SnO_2@NHPGC) anode

Co_1-Zn_9 NHPGC powder (5 mg) was dispersed in 40 ml of DI water by ultrasonication. Then, 15 mg of $SnCl_2 \cdot 2H_2O$ was added to the suspension and the mixture was sonicated short time and vigorously stirred at room temperature for 3 h. The resultant solution was filtered and dried at 80 °C in a vacuum oven. The dried powder was put into the tube furnace and heated at 350 °C with a heating rate of 5 °C min^{-1} under $Ar:H_2$ = 9:1 atmosphere for 3 h. After cooling to room temperature, SnO_2@NHPGC was obtained without further treatment.

Structural characterizations

The crystal structure was analyzed by the X-ray diffractometer (Smartlab, RIGAKU) with Cu-Kα radiation source at 1200 W (40 kV, 30 mA). Raman spectrometer (ARAMIS, Horiba Jobin Yvon) equipped with 514 nm Ar-ion laser and spot size of 1 μm was employed and acquisition and basic treatment of spectra were performed with LabSpec 5 software. X-ray photoelectron microscopy (XPS) spectra were obtained using K-alpha (Thermo VG Scientific) with Al-Kα radiation at beam current of 3 mA and beam size of 0.4 mm. The morphology and structure were observed using scanning electron microscope (SEM, JSM-7600F, JEOL) and double Cs-corrected transmission electron microscopy (TEM)/scanning TEM (STEM, ARM-200F, JEOL). The nitrogen adsorption-desorption isotherms and pore-size distributions were obtained by Quadrasorp (Quantachrome). The pore size distribution was determined by the non-local DFT (NLDFT) method and the Brunauer-Emmett-Teller (BET) surface area was calculated by the BET equation. The atomic ratio and the weight fraction were analyzed by the inductively coupled plasma optical emission spectroscopy (ICP-OES, Agilent) and the thermogravimetric analysis (TGA, Netzsch, TG 209 F3), respectively.

Operando characterization

The coin cell with a slit was used for X-ray penetration. SnO_2@NHPGC film on Cu foil and Li metal were used as a working electrode and a counter electrode. The coin cell was assembled with working and counter electrodes, minimal amounts of electrolyte, and punched separators in a center. The slit was sealed by mylar film and epoxy adhesive. The coin cell was galvanostatic cycled at a currend density of 50 mA g^{-1} and *operando* X-ray diffraction (XRD) patterns were obtained by D/MAX-2500 (Rigaku) every twenty minutes.

Fabrication and electrochemical characterizations of half cells

All the half cell tests were carried out using a 2032-type coin cell with a working electrode, and lithium or sodium metal as a reference and counter electrode. To fabricate the working electrode for a cathode, NHPGC, carbon black (Super-P) and polyvinylidene fluoride (PVDF) were mixed with a mass ratio of 8:1:1 in N-methyl-2-pyrrolidinone (NMP). Then, the obtained mixture was casted on carbon fiber paper and dried at 80 °C in a vacuum oven. For the anode test, SnO_2@NHPGC, Super-P, and PVDF were mixed in 7:2:1 in NMP and casted on copper foil. The typical mass loading was 2.5 mg cm^{-2} for the cathode and 1 mg cm^{-2} for the anode. The coin cell was assembled in argon-filled glove box with a polypropylene separator (Celgard 2400) and electrolyte of 1 M $LiPF_6$ in ethylene carbonate (EC) and diethyl carbonate (DEC) (1:1 v/v). In case of sodium-ion half cell, a glass fiber separator (GF-D) and 1 M $NaClO_4$ in EC/DEC (1:1 v/v) electrolyte were employed. Cyclic voltammetry (CV) and galvanostatic charge/discharge (GCD) tests were measured on a battery cycler (Wonatech, WBCS-3000). The galvanostatic intermittent titration technique (GITT) curves were obtained at the 2nd cycle with a pulse current of 100 mA g^{-1} for 10 min of a pulse time and 10 min of a relaxation time. The diffusion coefficient of Li ion (D_{Li}) is calculated from the following equation of

$$D = 4/\pi\tau \times (m_B V_M/M_B S)^2 \times (\Delta E_S/\Delta E_\tau)^2 \qquad (S1)$$

where m_B is the mass of active materials, V_M is the molar volume, M_B is the molecular weight, S is the electrode surface area, τ is the pulse time, ΔE_s is the voltage change between steady-state, and ΔE_τ is the voltage change during constant current pulse subtracting iR drop.

Fabrication of electric double layer capacitors (EDLCs)

To further investigate the electrochemical behaviors of NHPGC as a capacitor-type cathode, the EDLC in symmetric configuration was fabricated for the electrochemical impedance spectroscopy (EIS) measurement. The working electrode was produced with the same procedure to the cathode half-cell. Then, the symmetric EDLC coin cell was fabricated with two working electrodes face-to-face and a glass fiber separator (GF-D) between them. 1 M $TEABF_4$ in acetonitrile was employed as an electrolyte. The electrochemical impedance spectroscopy (EIS) measurement was carried out using the potentiostat (VSP, Biologic).

Fabrication and electrochemical characterizations of hybrid energy storage (HES) cells

The HES cell was assembled using NHPGC as a cathode and SnO_2@NHPGC as an anode. Before fabrication of the full cell, SnO_2@NHPGC anode was pre-lithiated (or pre-sodiated) to 0.05 V at a current density of 0.1 A g^{-1}. Then, the HES cell was assembled with the pre-lithiated (or pre-sodiated) SnO_2@NHPGC anode and NHPGC cathode in the Ar-filled glove box. The mass ratio of cathode and anode was set to be 2.5:1 and 2:1 for Li-ion HES and Na-ion HES, respectively, which were optimized to balance the total charge on each electrode. The electrochemical measurements of the HES were conducted on the same method as the half cell tests. Energy density (E, Wh kg^{-1}) and power density (P, W kg^{-1}) were calculated by the following equations of

$$P = V \times i/m \quad \text{(S2)}$$

$$E = P \times t/3600 \quad \text{(S3)}$$

$$V = (V_{max}+V_{min})/2 \quad \text{(S4)}$$

where V, i, and t are the voltage window, current, and discharge time of the HES, m is the total mass of the active materials of cathode and anode, and V_{max} and V_{min} are the maximum and minimum voltage during the discharge.

Ultrafast charging module demonstration

An ultrafast charging module consists of the HES cell part, the photovoltaic solar cell part for charging, and the mini-motor operating part with the windmill model. Three NHPGC//SnO_2@NHPGC Li-ion HES cells are connected and charged by the solar cell when the light is irradiated. The solar cell leads to the 5 V maximum voltage leading to 65 mA current under the 100 mW cm^{-2} AM 1.5 G and the mini-motor operates only when switched on.

Section S2. Supporting figures and tables

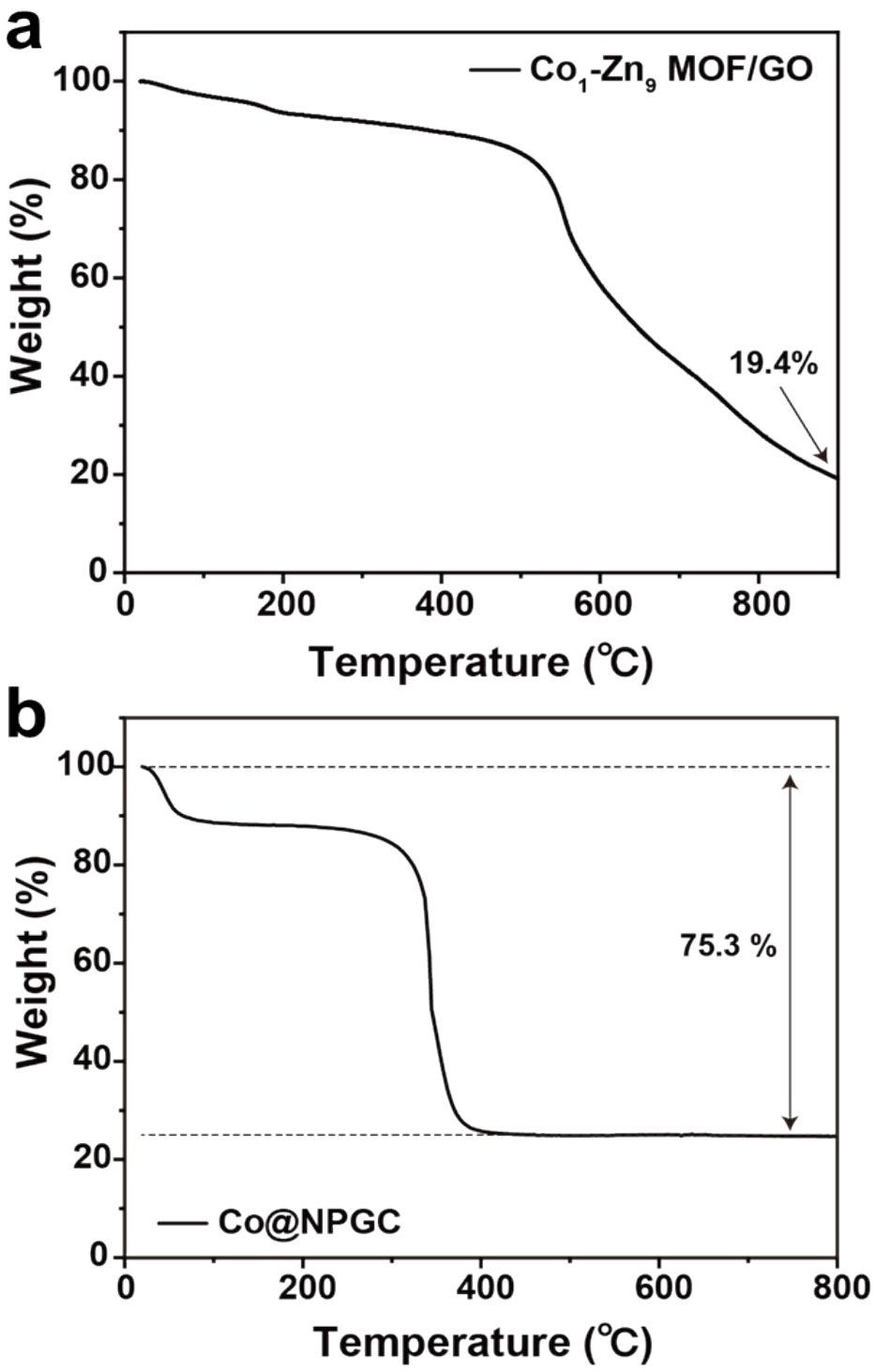

Figure S1. TGA curves of Co_1-Zn_9 MOF/GO and Co@NPGC (Co_1-Zn_9 NHPGC. TGA data of (a) Co_1-Zn_9 MOF/GO at N_2 atmosphere and (b) Co@NPGC (Co_1-Zn_9 NHPGC before acid treatment) at air atmosphere.

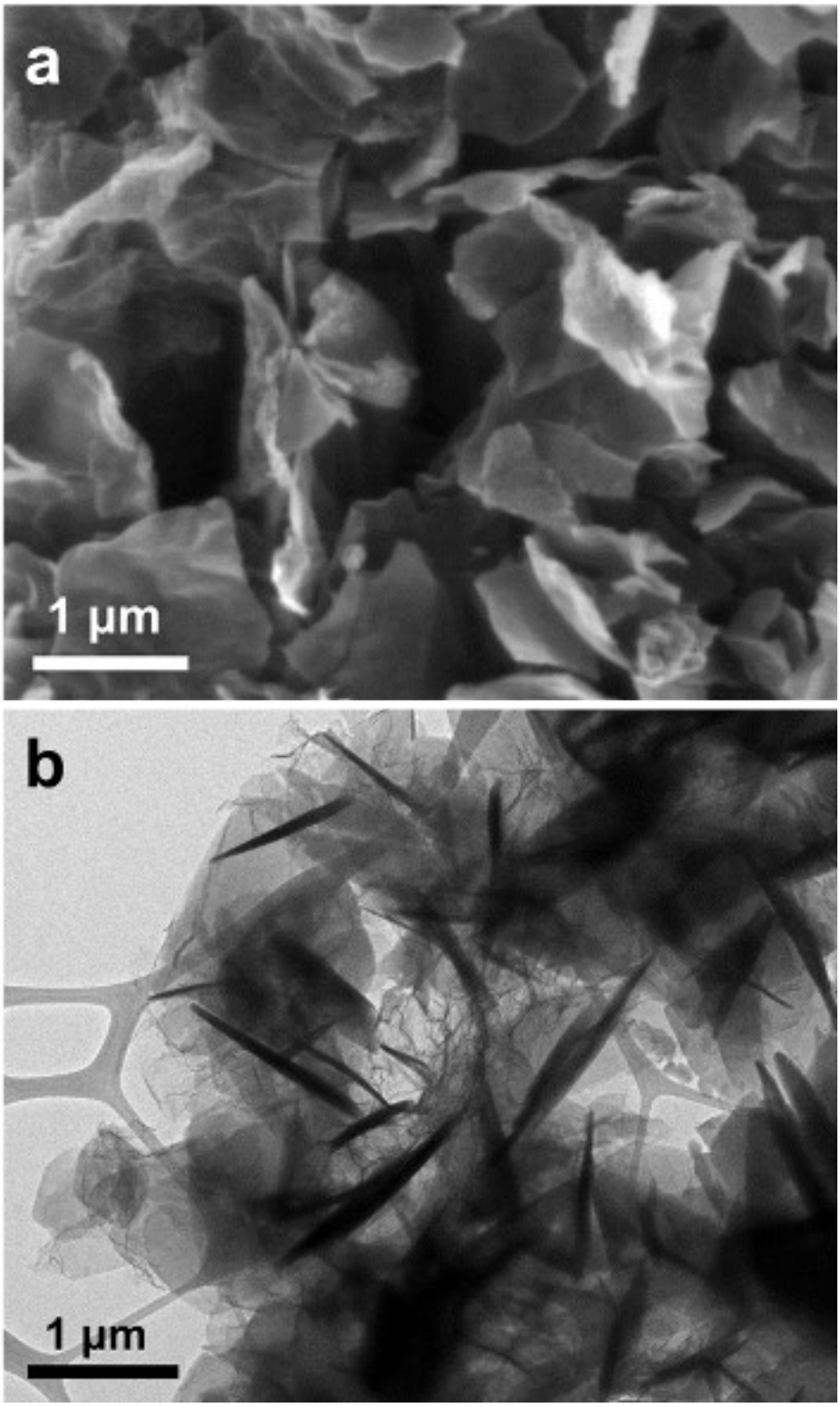

Figure S2. Structural characterizations of Co_1-Zn_9 MOF/GO. (a) SEM and (b) TEM images of Co_1-Zn_9 MOF/GO.

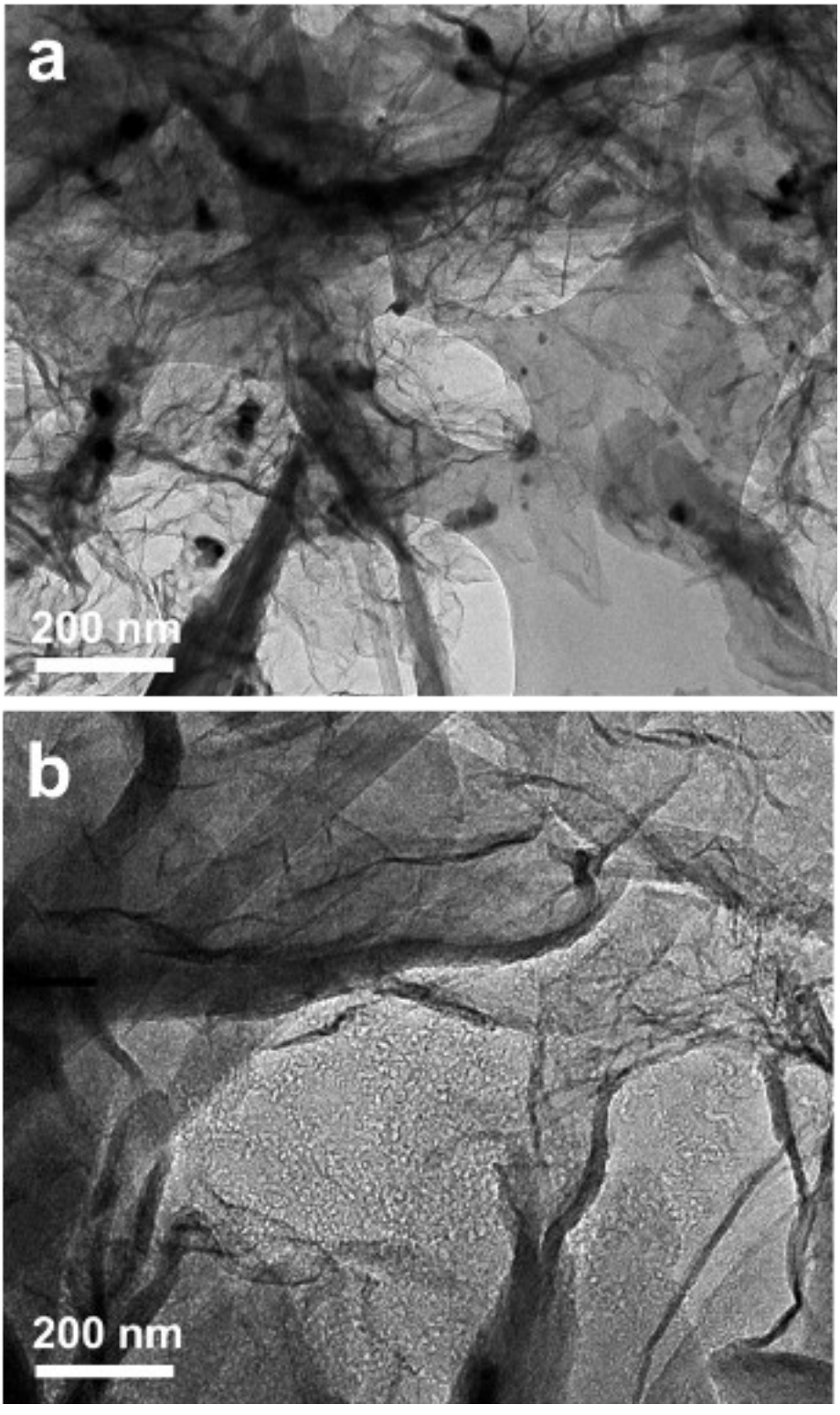

Figure S3. Structural characterizations of Co@NPGC and Co_1-Zn_9 NHPGC. TEM images of (a) Co@NPGC before acid treatment and (b) Co_1-Zn_9 NHPGC after Co removal by acid treatment.

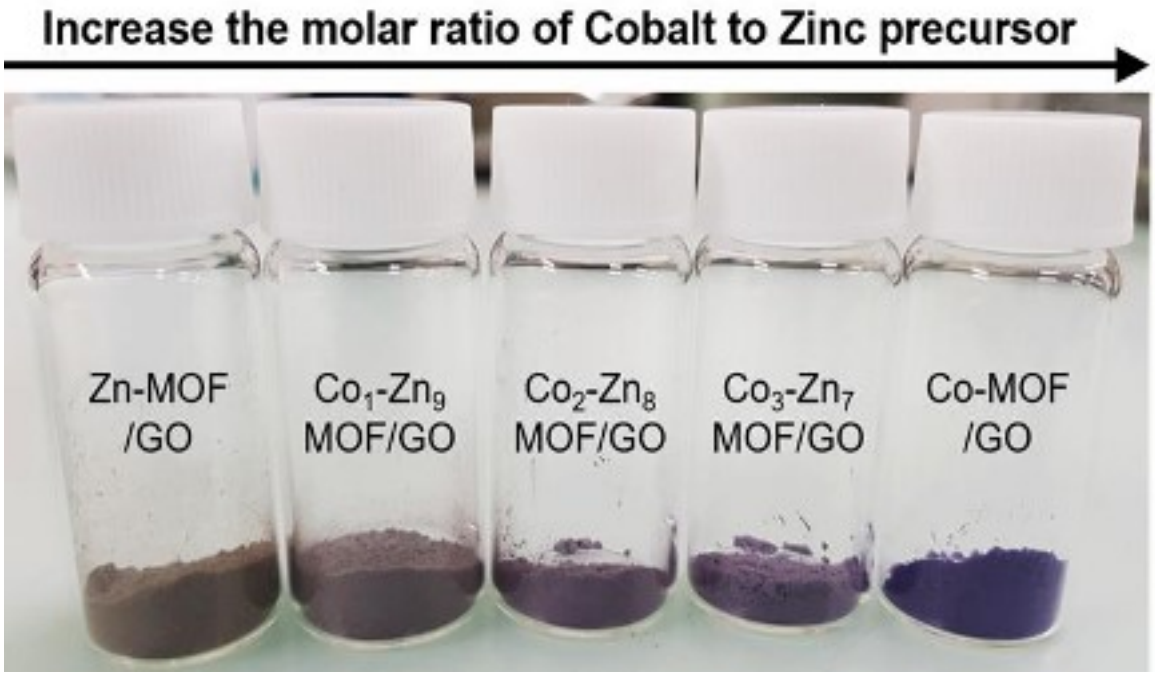

Figure S4. Color changes of Co_x-Zn_{10-x} MOF/GO samples.

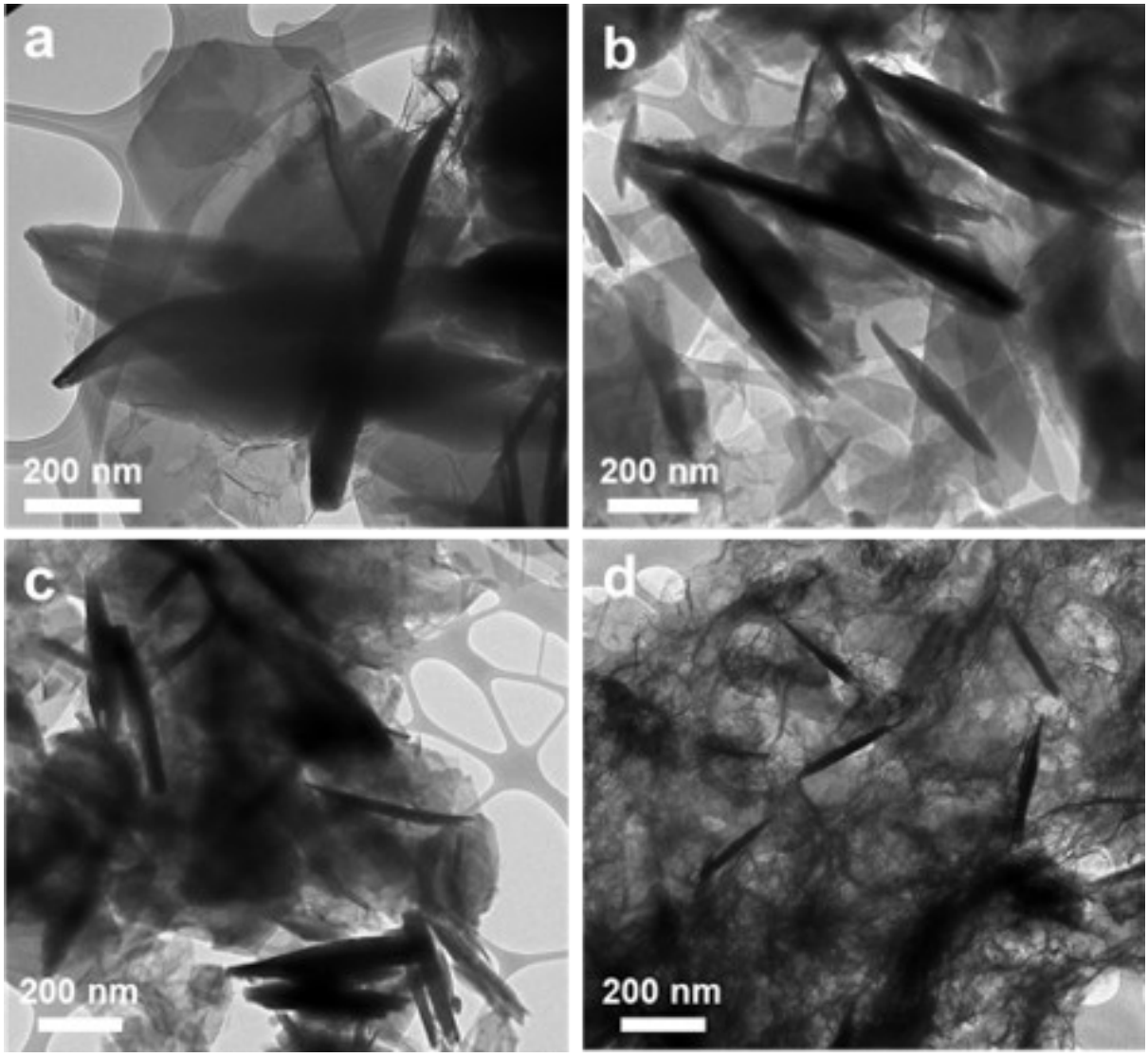

Figure S5. Structural characterizations of Co_x-Zn_{10-x} NHPGC structures. TEM images of (a) Zn-NHPGC, (b) Co_2-Zn_8 NHPGC, (c) Co_3-Zn_7 NHPGC, and (d) Co-NHPGC.

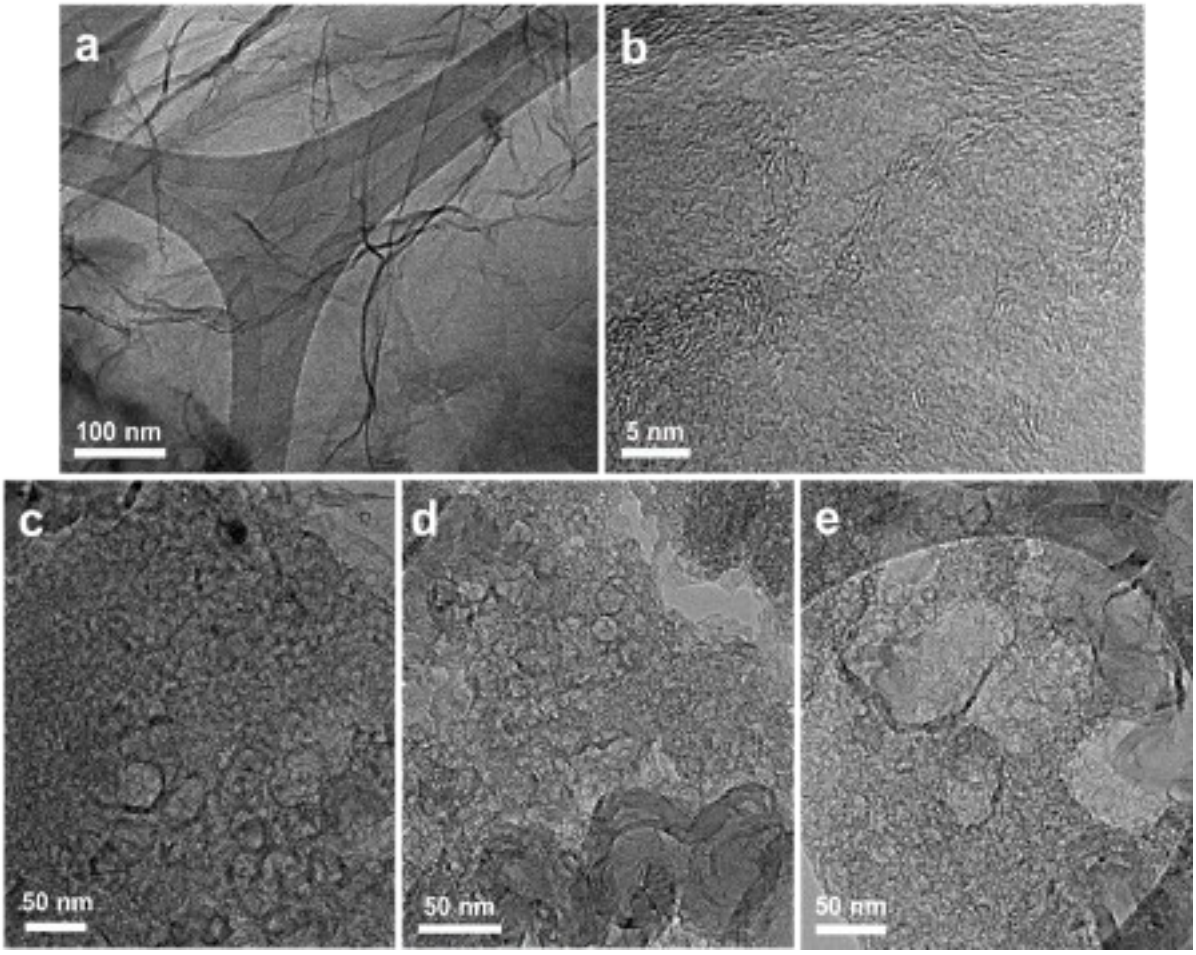

Figure S6. TEM and high-resolution TEM (HRTEM) images of Co_x-Zn_{10-x} NHPGC. (a) TEM and (b) HRTEM images of Zn-NHPGC. TEM images of (c) Co_2-Zn_8 NHPGC, (d) Co_3-Zn_7 NHPGC, and (e) Co-NHPGC.

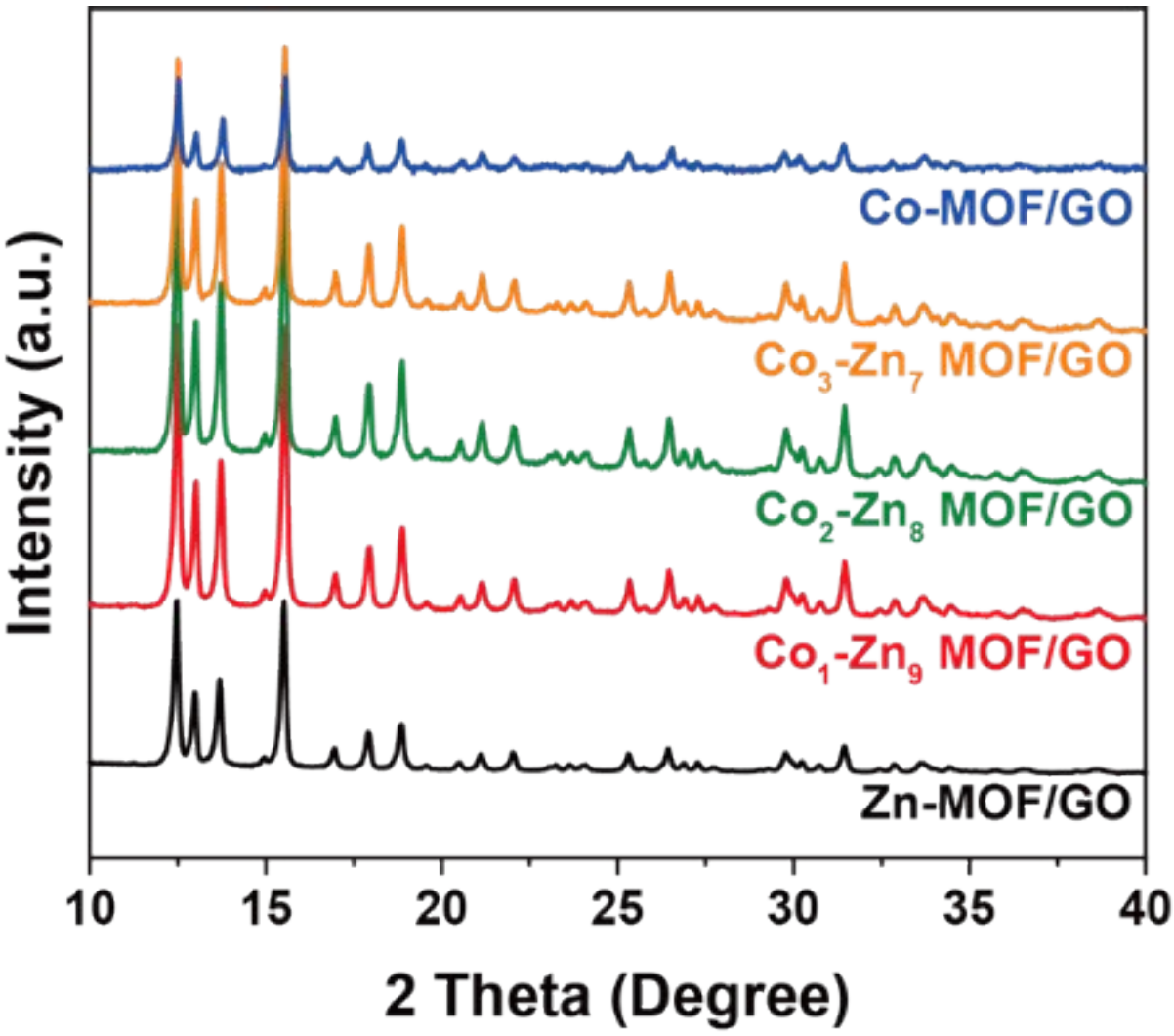

Figure S7. XRD spectra of Co_x-Zn_{10-x} MOF/GO.

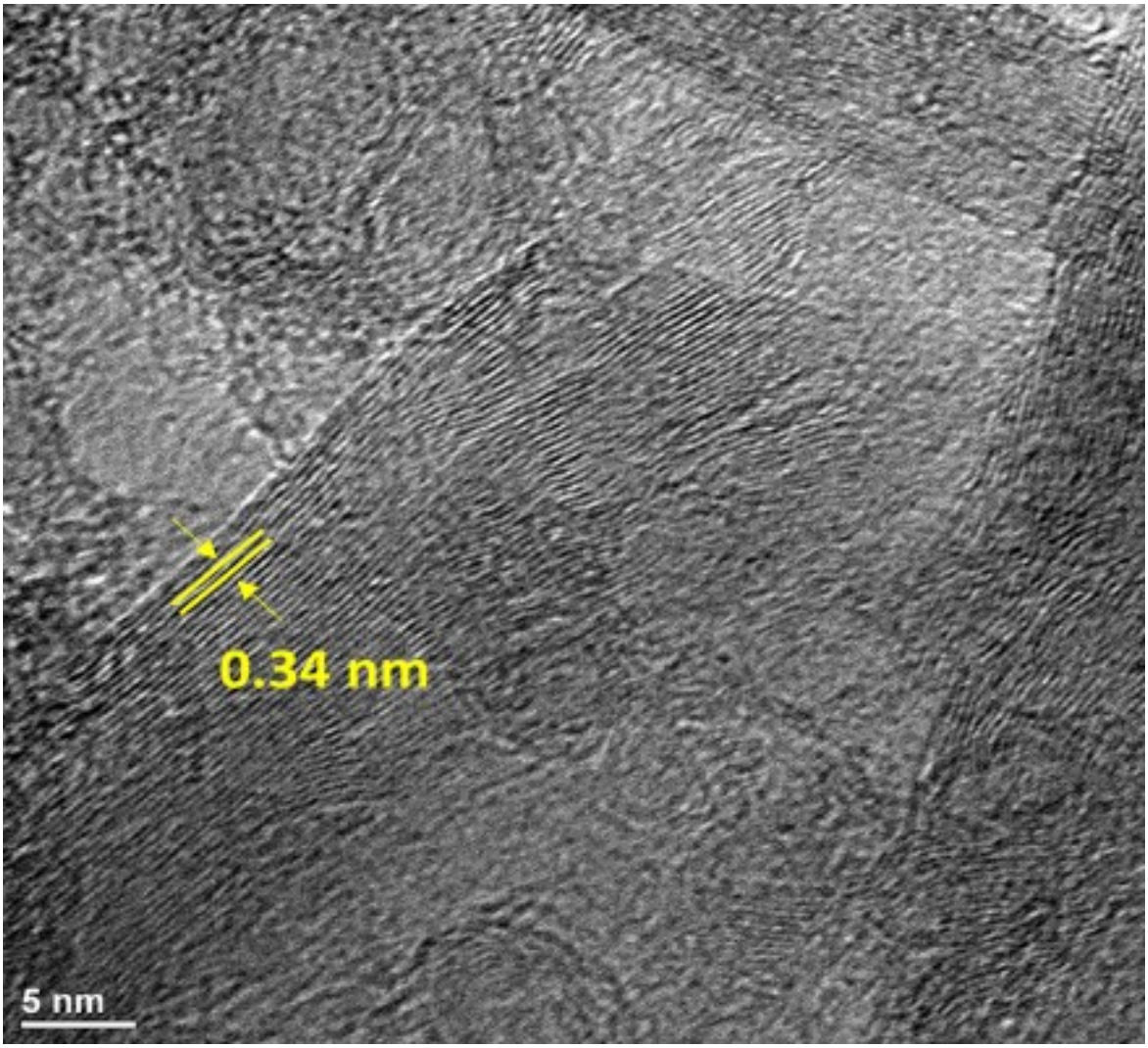

Figure S8. HRTEM image of Co-NHPGC. The lattice spacing of carbon layers is 0.34 nm, corresponding to highly graphitic structure.

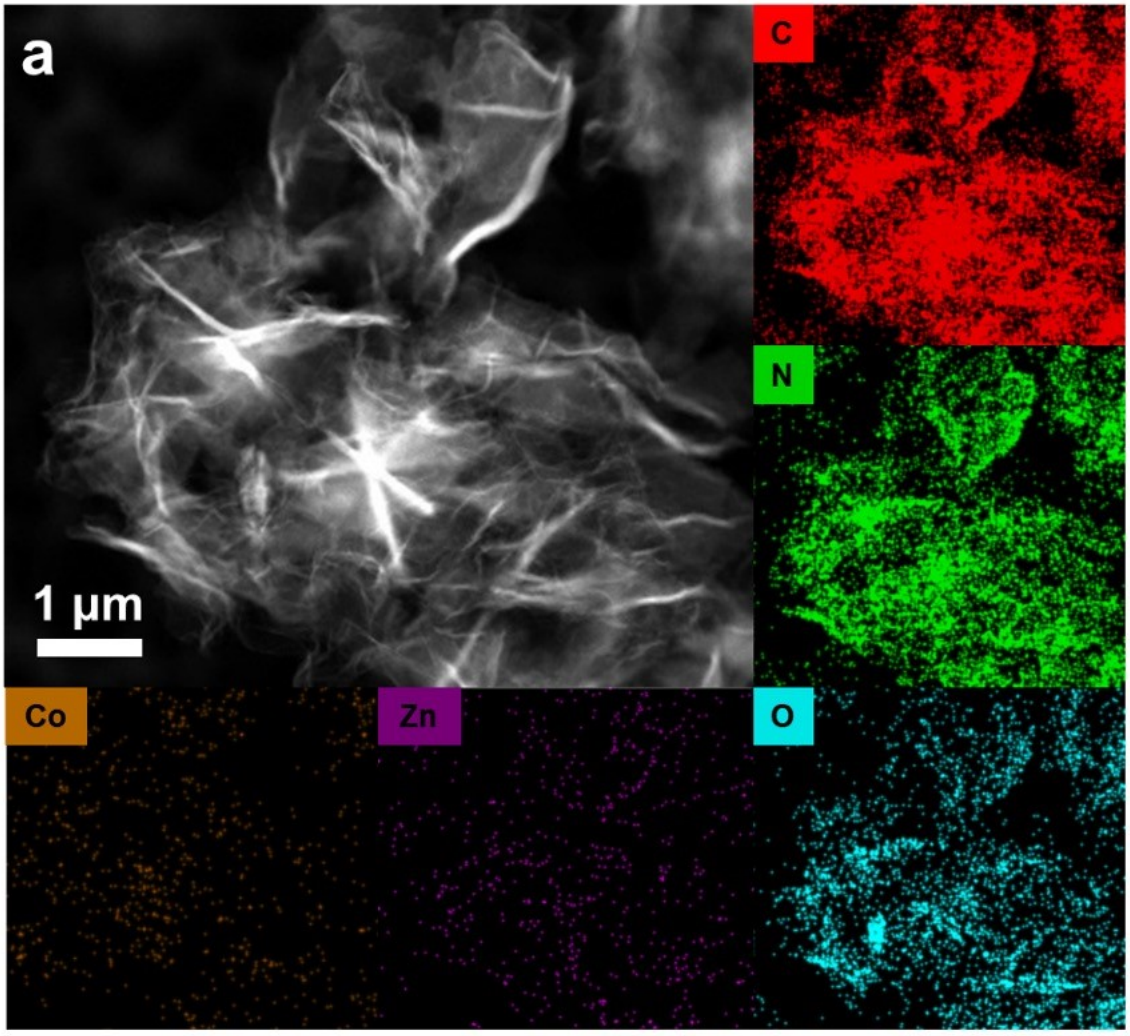

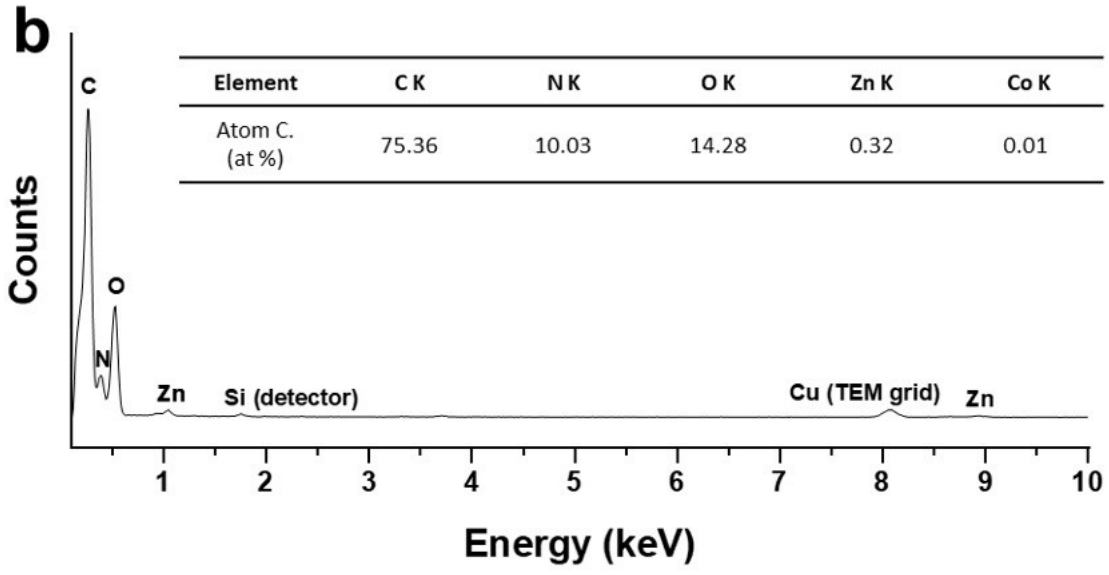

Figure S9. TEM image and energy dispersive spectroscopy (EDS) spectra. (a) TEM image and (b) EDS spectra of Co_1-Zn_9@NHPGC.

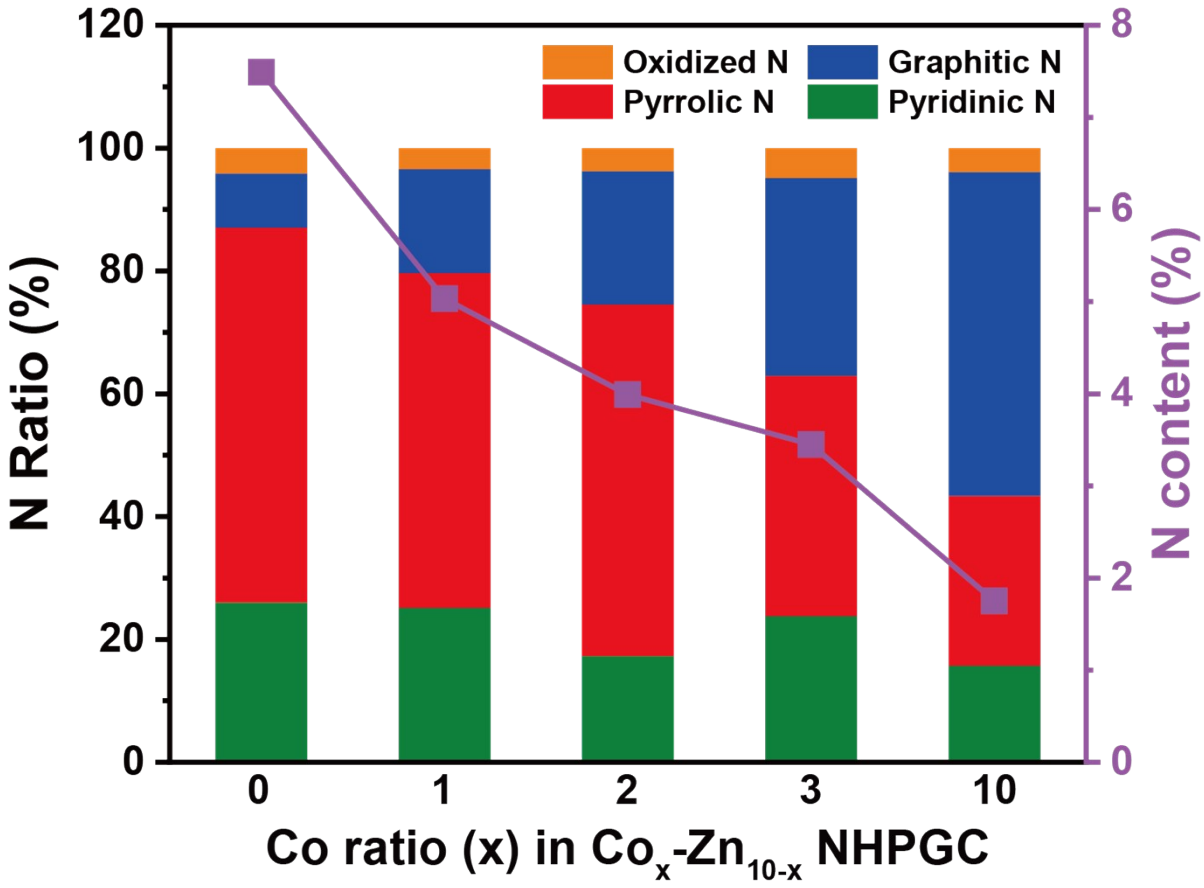

Figure S10. Area ratio depending on nitrogen doping types and total nitrogen contents of Co_x-Zn_{10-x} NHPGC calculated from XPS N 1s spectra.

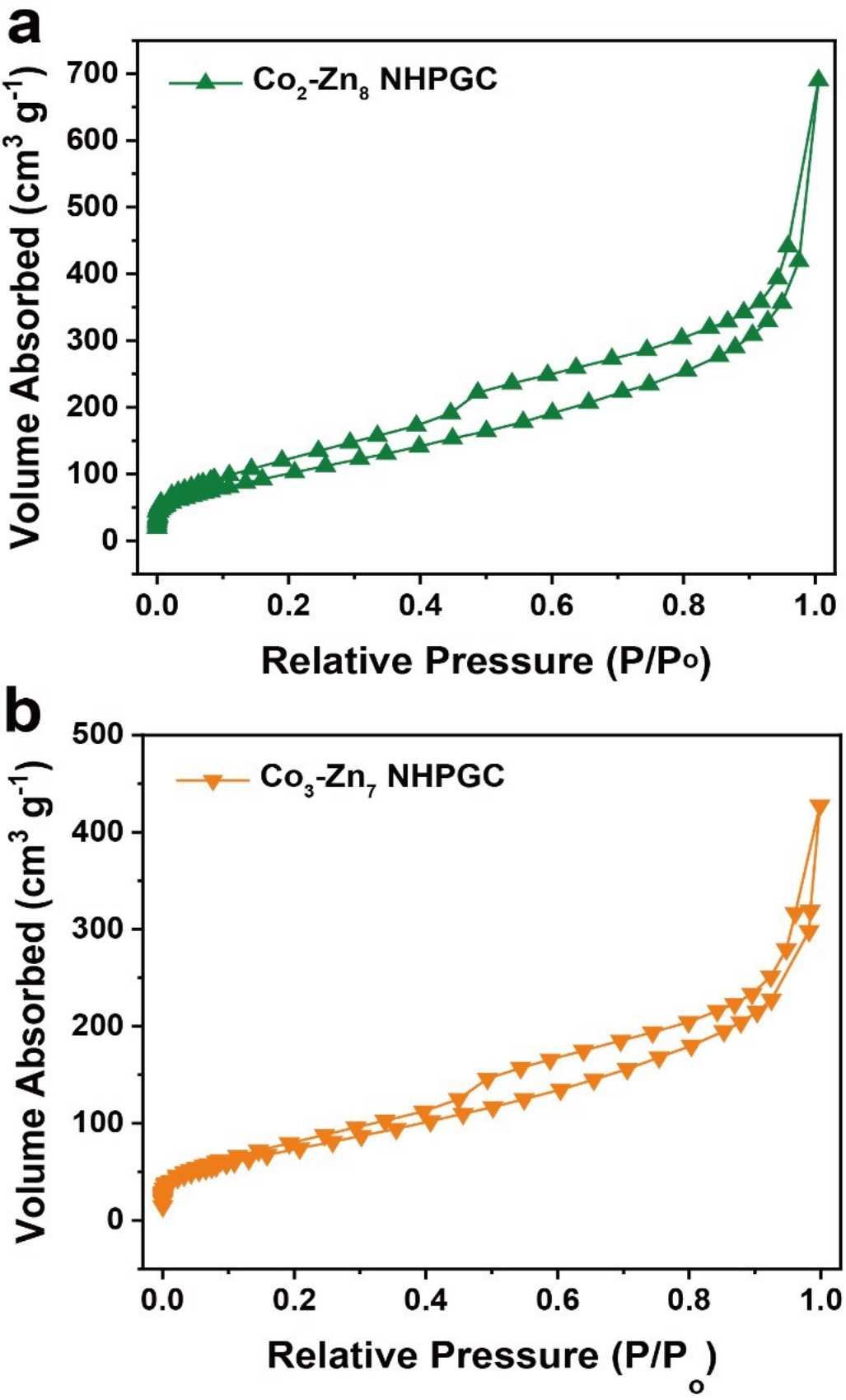

Figure S11. N_2 adsorption isotherm. Those for (a) Co_2-Zn_8 and (b) Co_3-Zn_7 NHPGCs

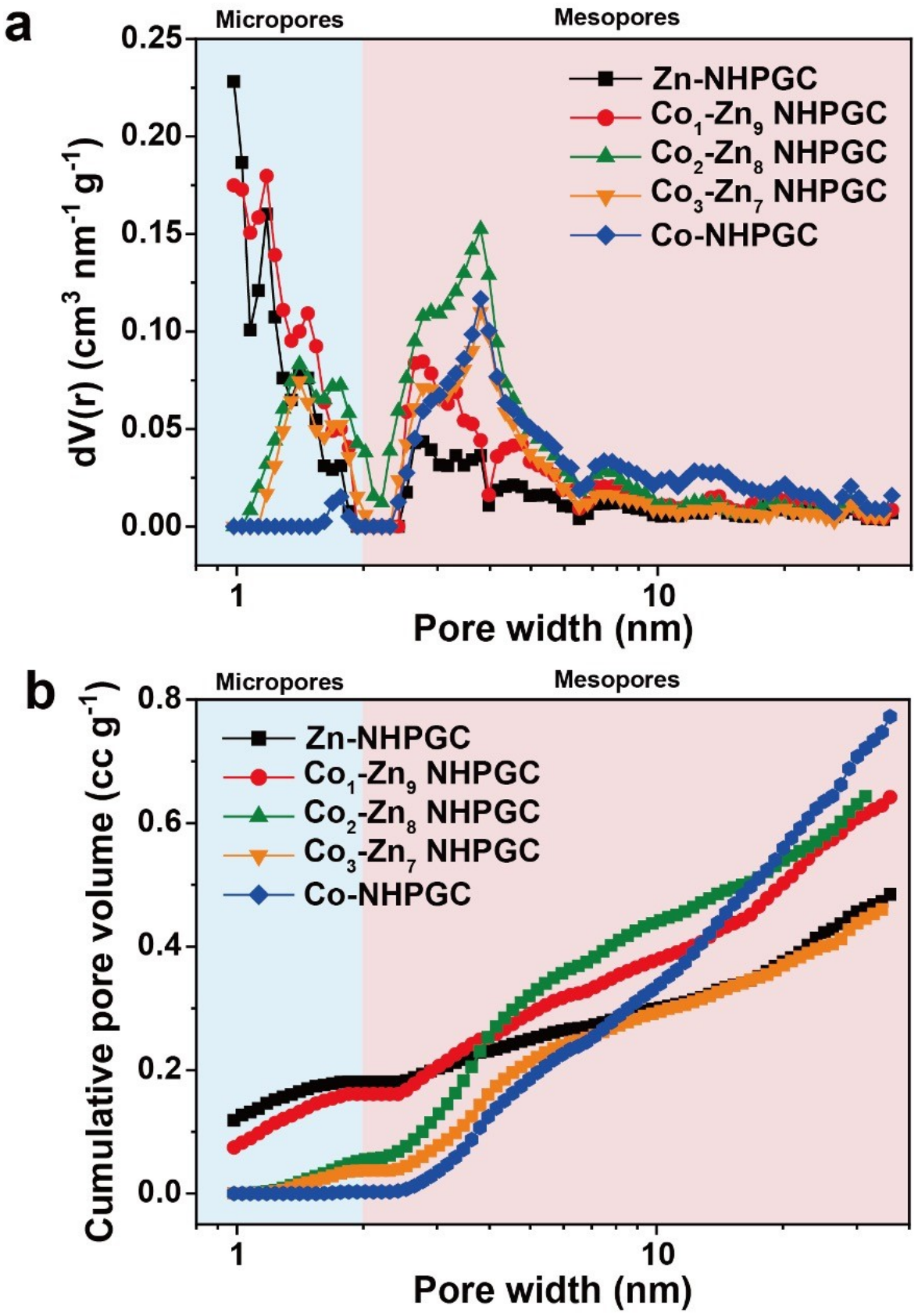

Figure S12. Pore size and volume characteristics of Co_x-Zn_{10-x} NHPGCs. (a) Pore size distribution and (b) cumulative pore volume of Co_x-Zn_{10-x} NHPGCs.

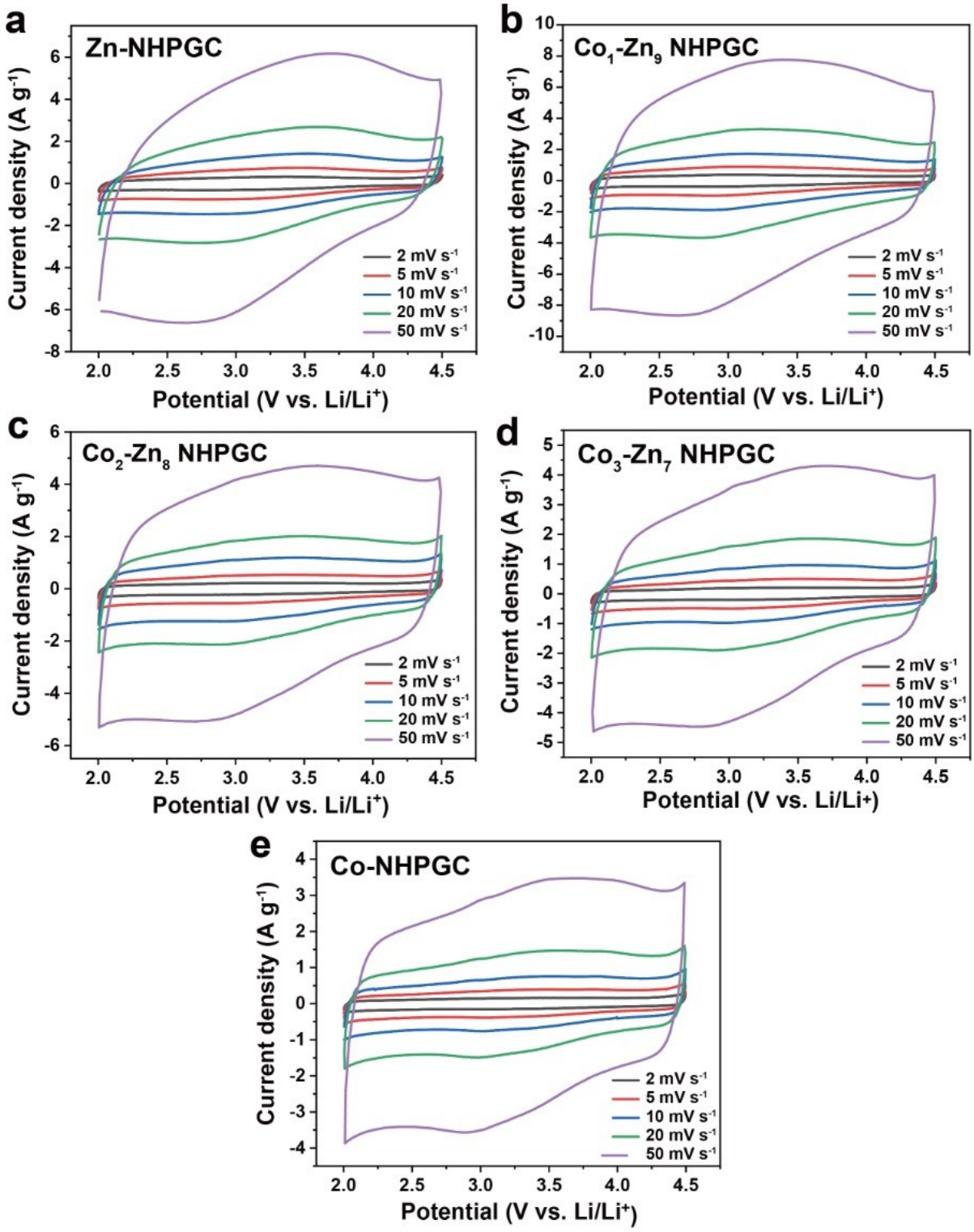

Figure S13. CV curves of Co_x-Zn_{10-x} NHPGC structures. Those of (a) Zn-NHPGC, (b) Co_1-Zn_9 NHPGC, (c) Co_2-Zn_8 NHPGC, (d) Co_3-Zn_7 NHPGC, and (e) Co-NHPGC in $LiPF_6$ electrolyte at various scan rates.

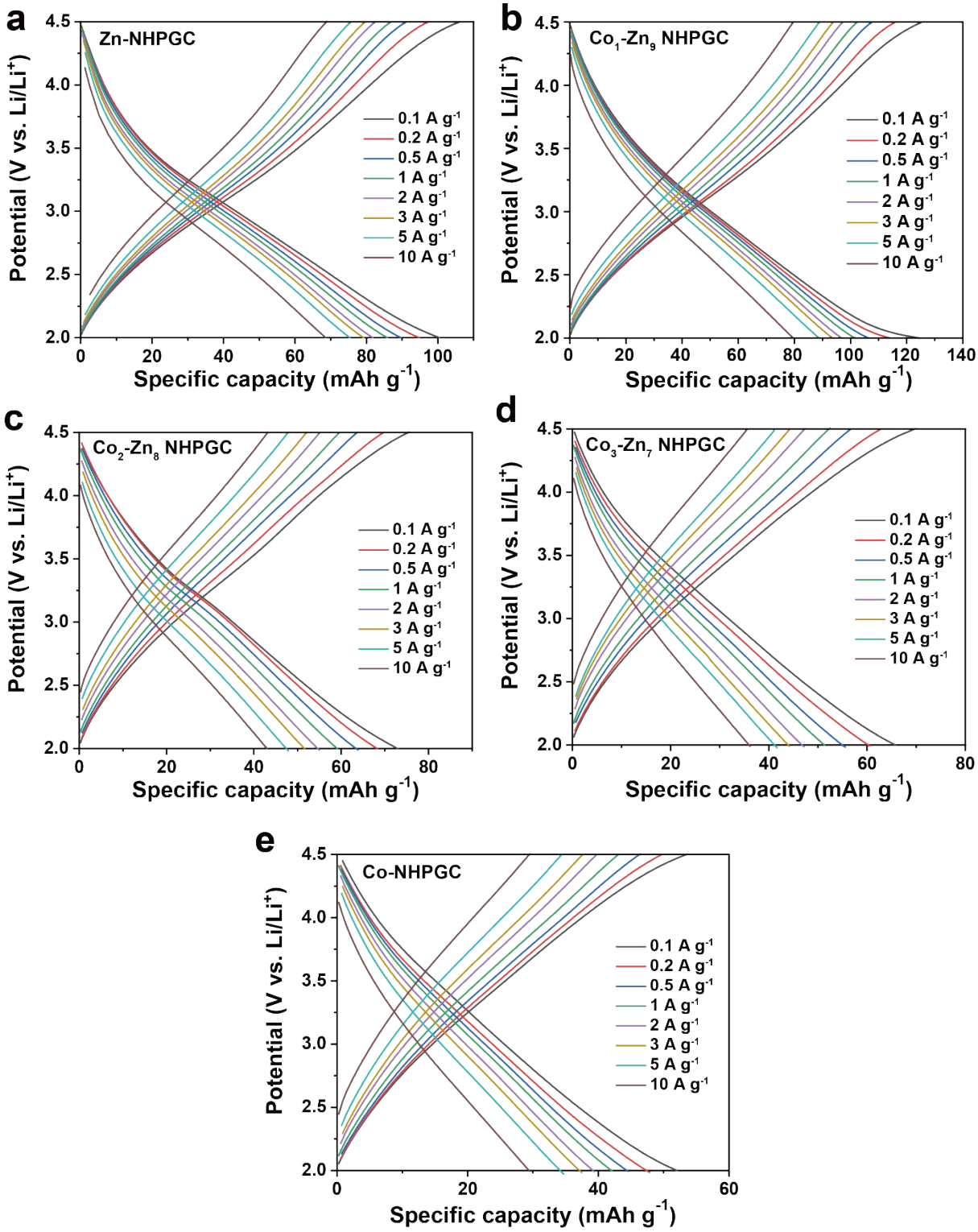

Figure S14. GCD curves of Co_x-Zn_{10-x} NHPGC structures. Those of (a) Zn-NHPGC, (b) Co_1-Zn_9 NHPGC, (c) Co_2-Zn_8 NHPGC, (d) Co_3-Zn_7 NHPGC, and (e) Co-NHPGC in $LiPF_6$ electrolyte at different current densities.

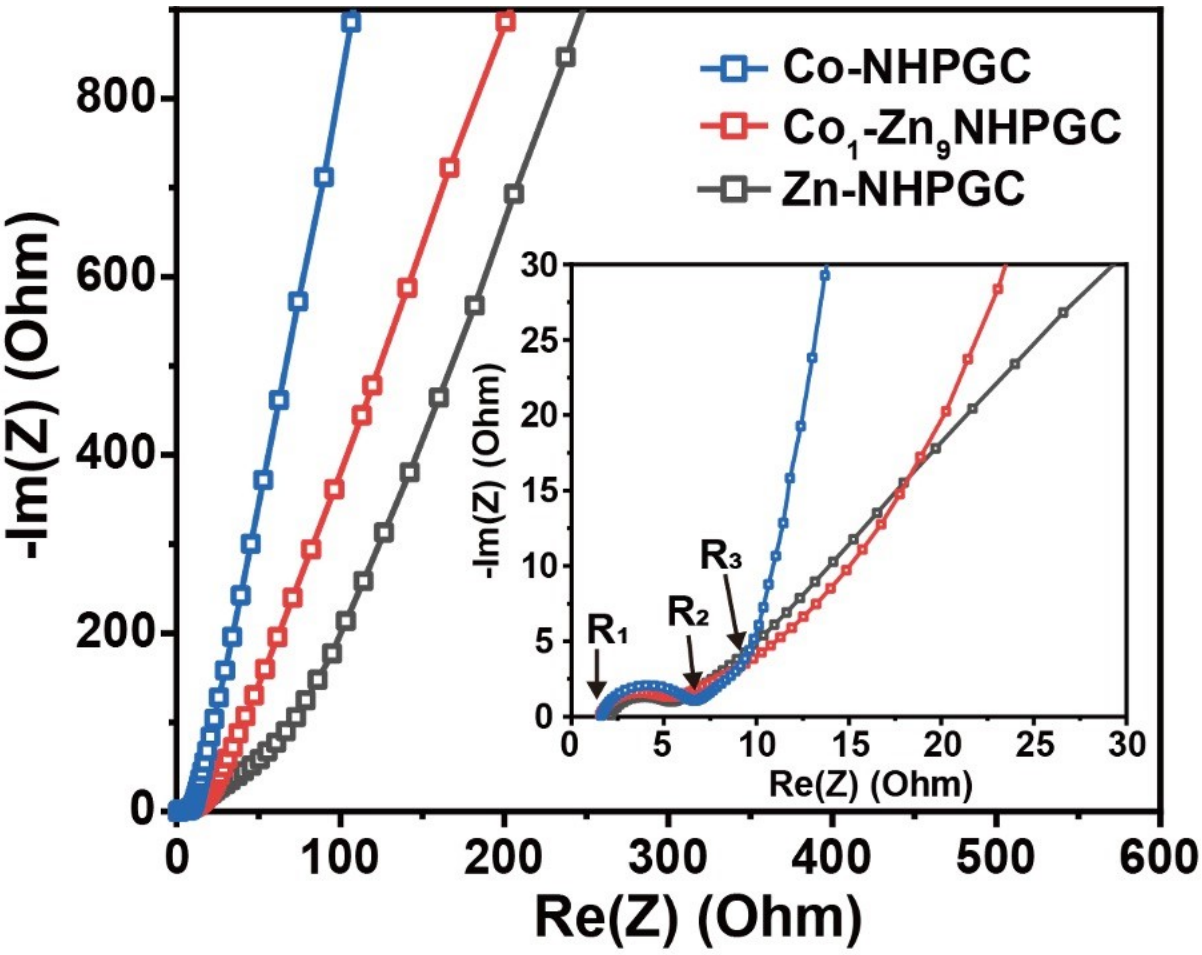

Figure S15. Nyquist plot of Zn-NHPGC, Co_1-Zn_9 NHPGC, and Co-NHPGC.

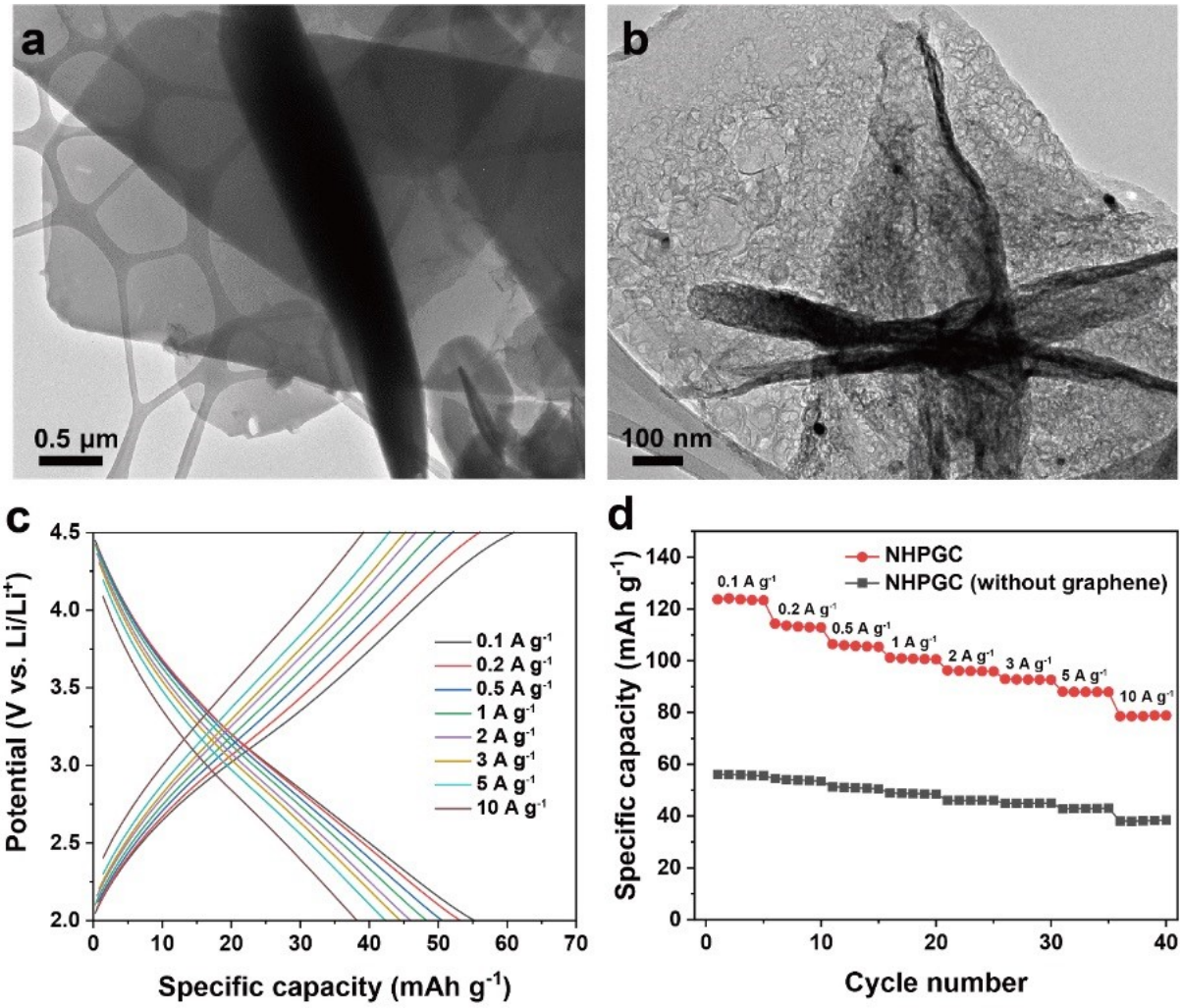

Figure S16. TEM image and electrochemical performances of Co_1-Zn_9 MOF without GO or graphene. TEM images of (a) Co_1-Zn_9 MOF without GO and (b) NHPGC without graphene after carbonization. (c) Rate performances and (D) GCD curves of NHPGC and NHPGC without graphene.

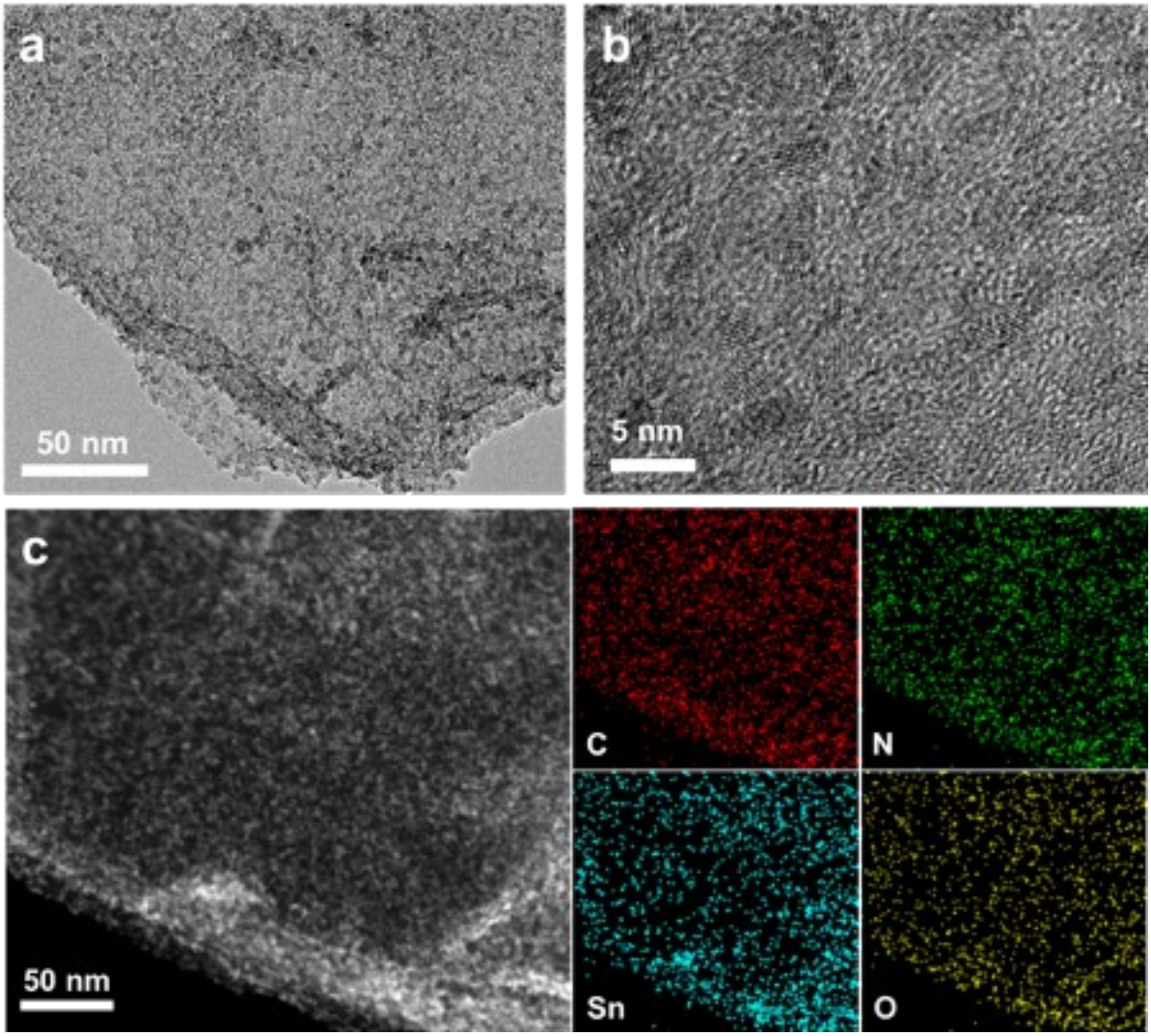

Figure S17. TEM and high-angle annular dark-field scanning TEM (HAADF-STEM) images. TEM images at (a) low and (b) high magnification, and (c) HAADF-STEM images with EDS-mapping of SnO_2@NHPGC.

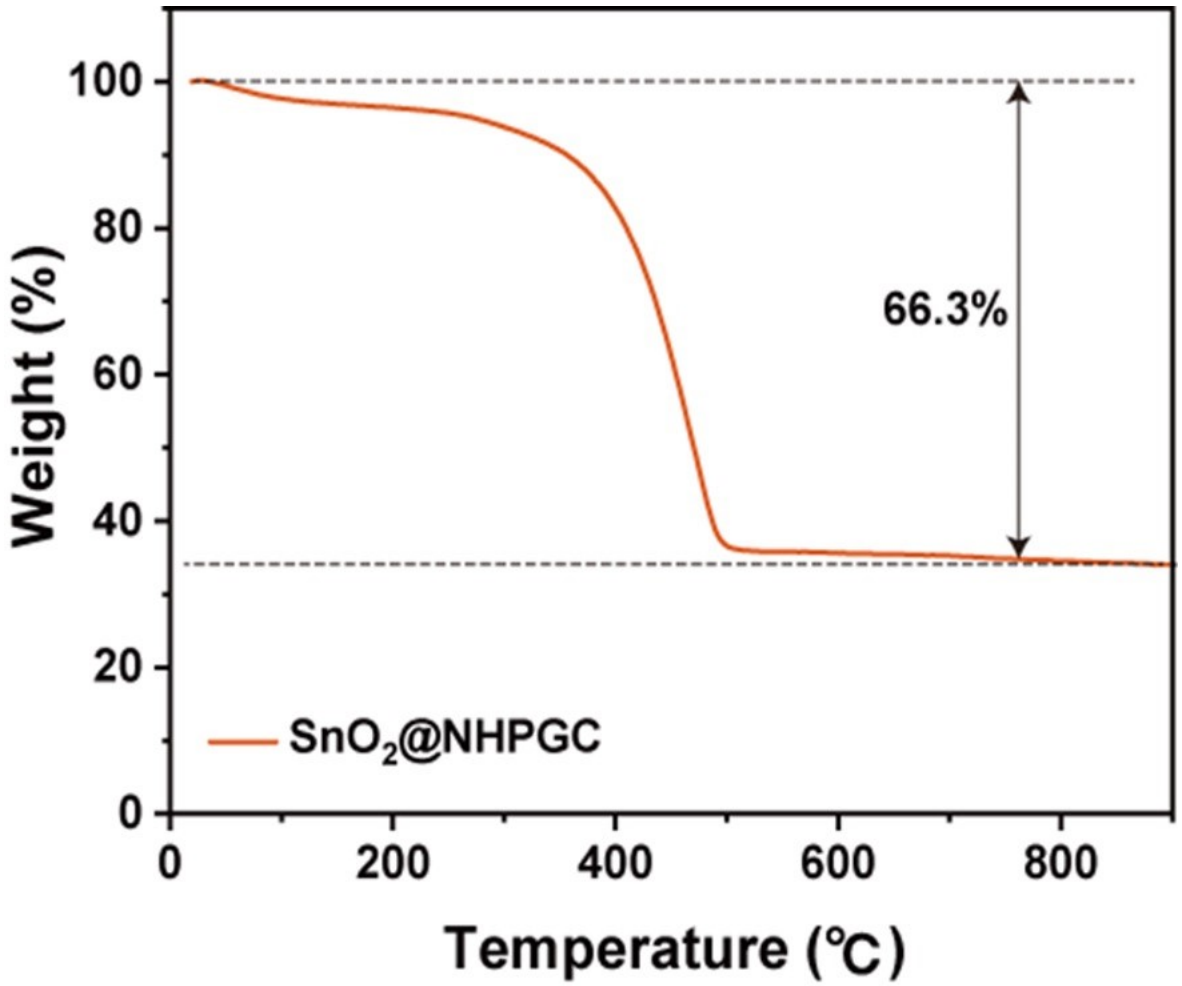

Figure S18. TGA of SnO_2@NHPGC in air atmosphere.

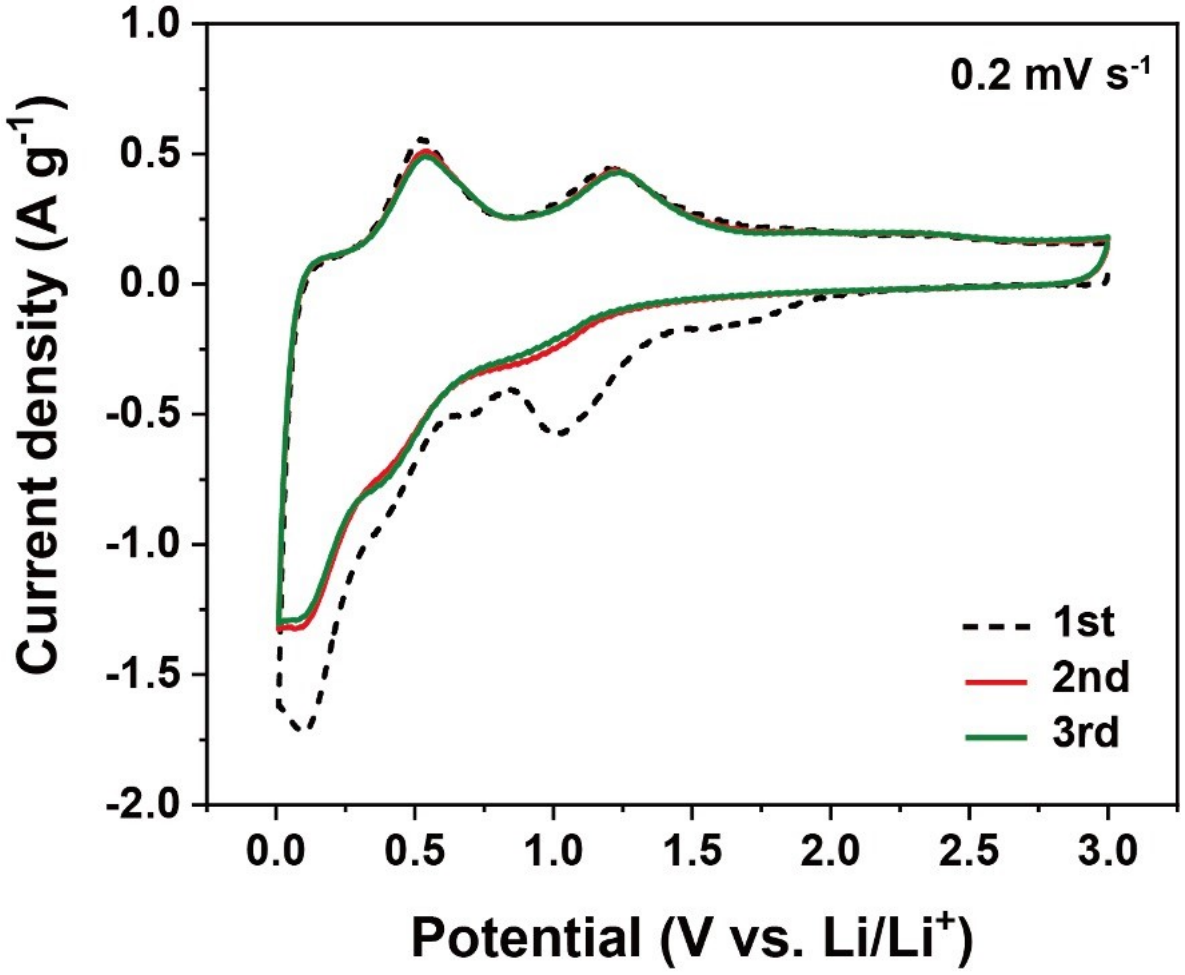

Figure S19. CV curves of the initial three cycles of SnO_2@NHPGC anode at a scan rate of 0.2 mV s^{-1}.

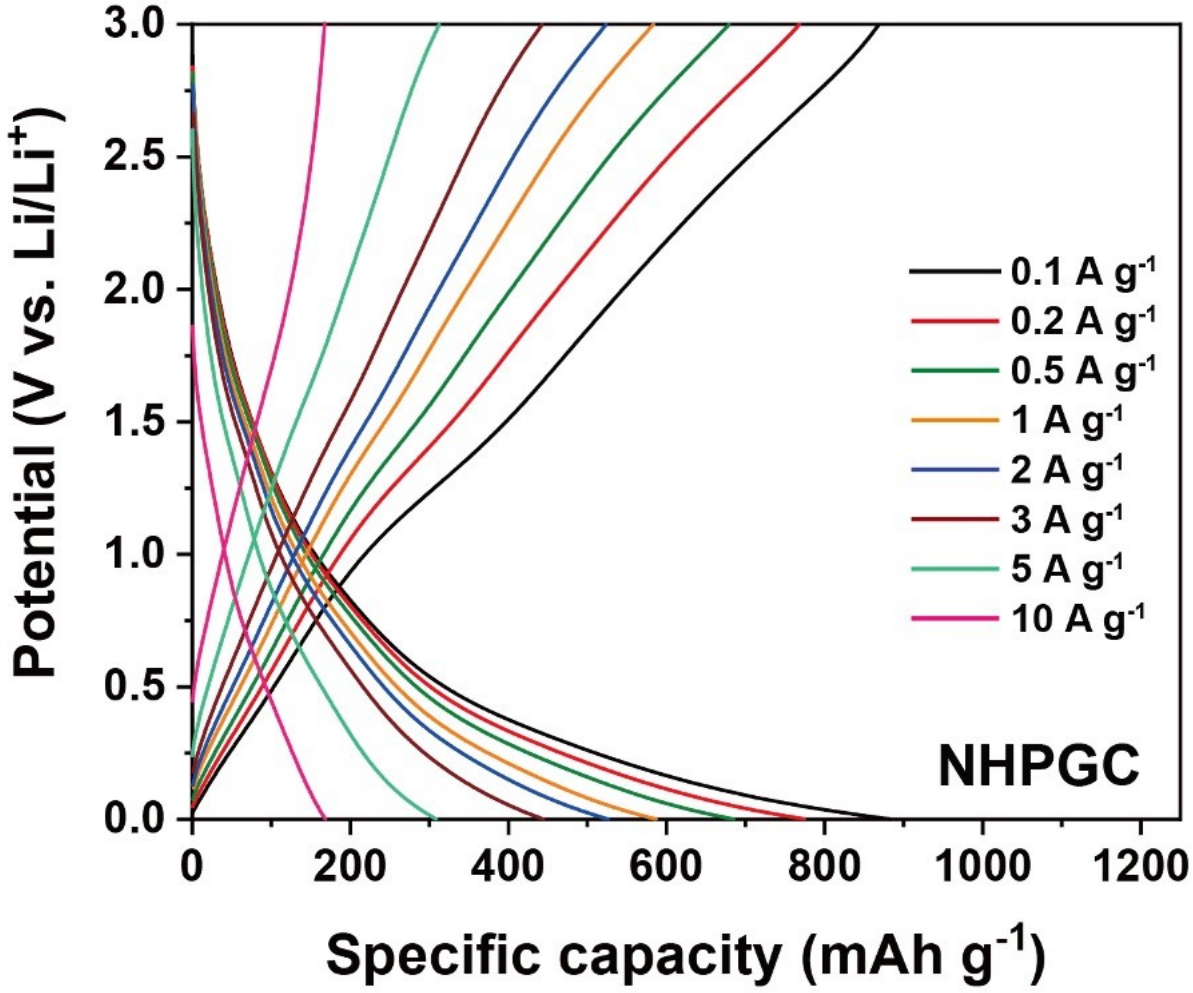

Figure S20. GCD curves at different current densities of NHPGC anode.

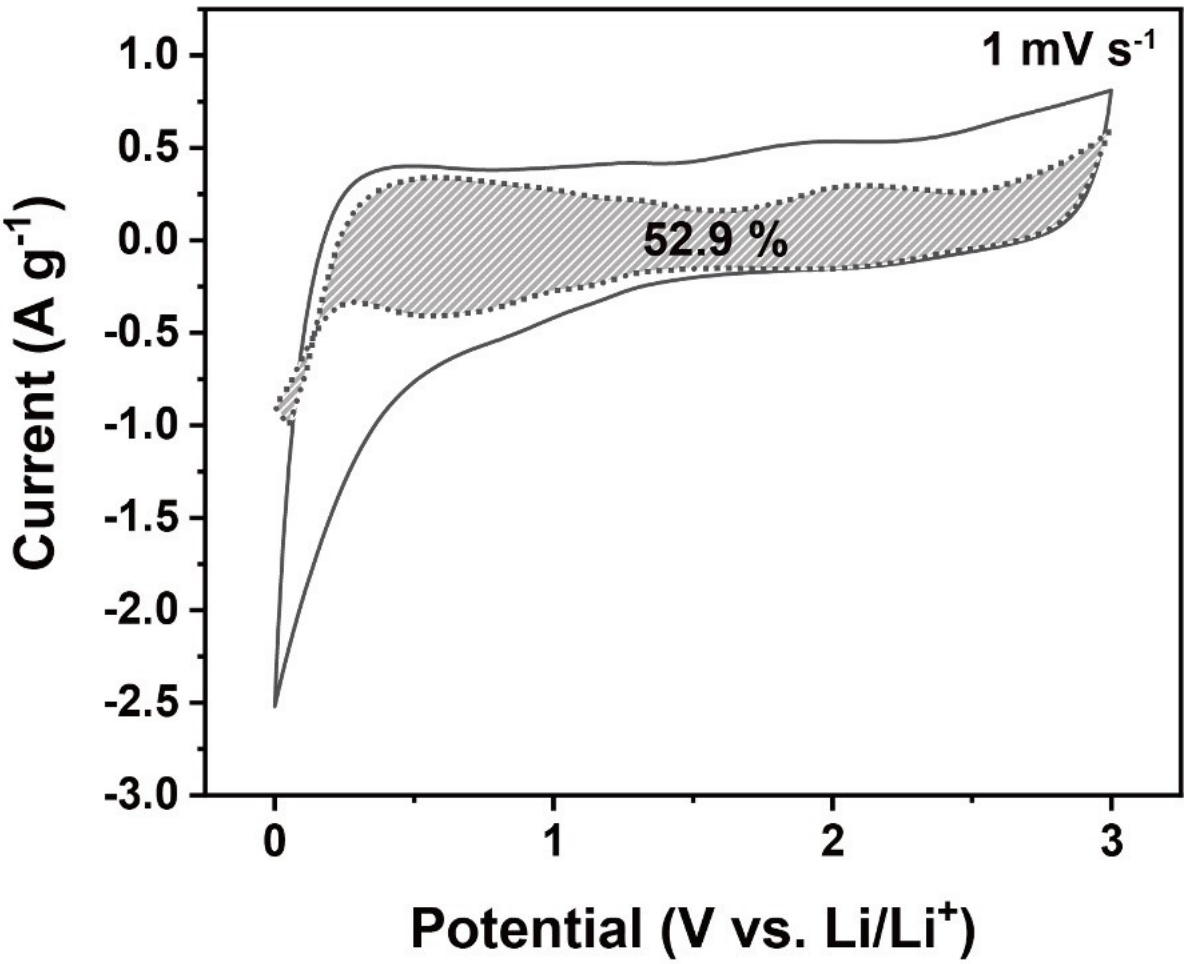

Figure S21. Capacitive contribution for NHPGC anode.

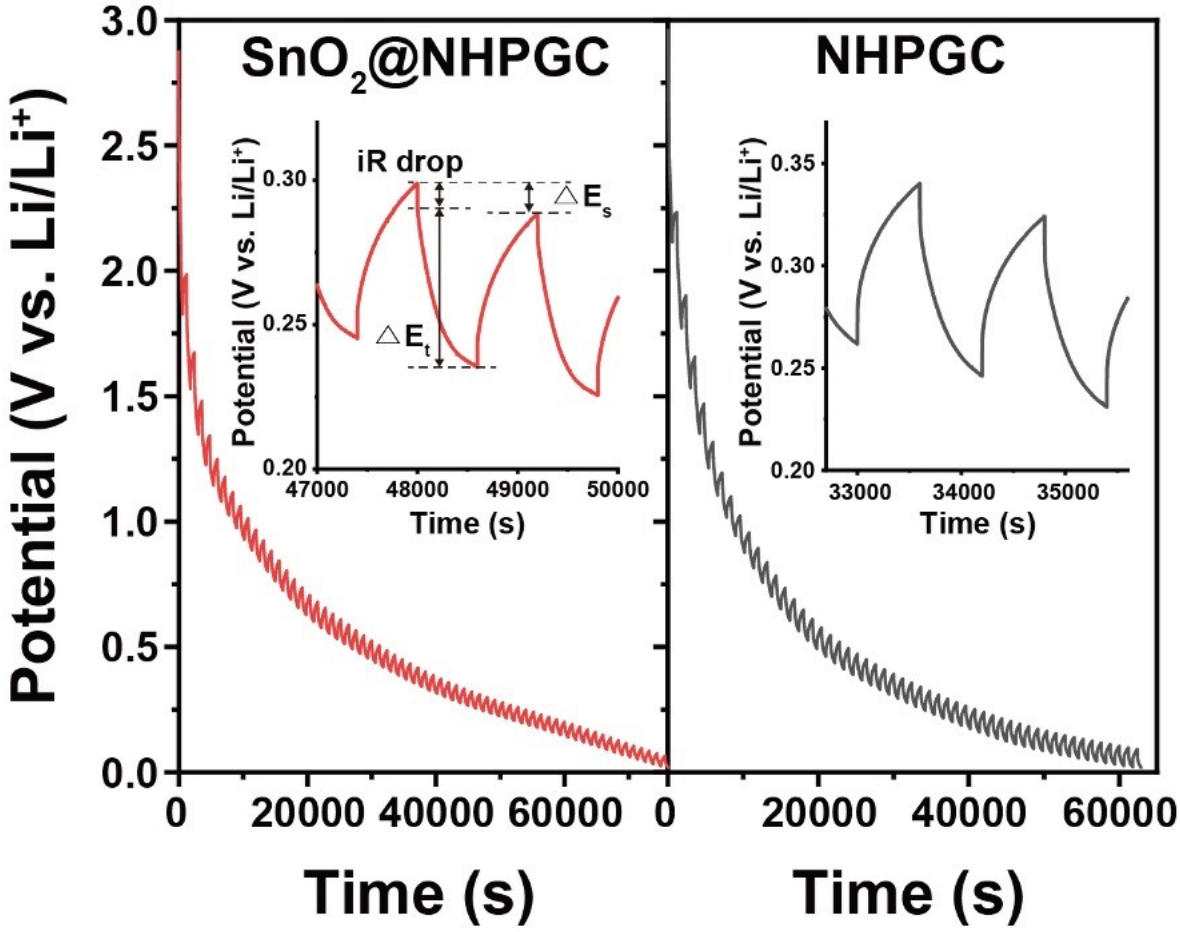

Figure S22. GITT curves of SnO_2@NHPGC and NHPGC anodes in $LiPF_6$.

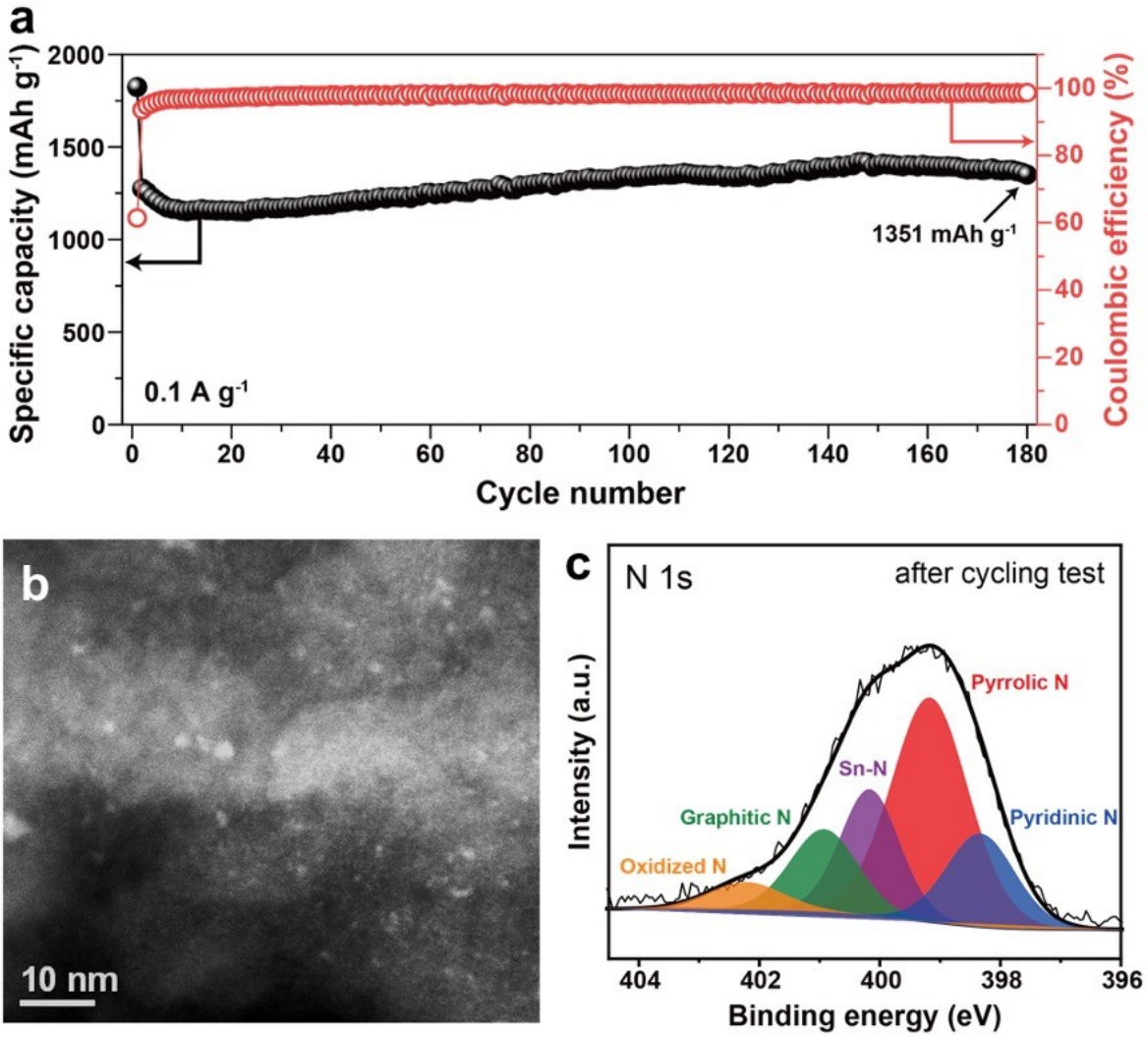

Figure S23. Cycling performance and structural characteristics after cycling. (a) Galvanostatic cycling of SnO_2@NHPGC at 100 mA g^{-1}. (b) HAADF-STEM image and (c) XPS N 1s spectra of SnO_2@NHPGC after 180 cycles.

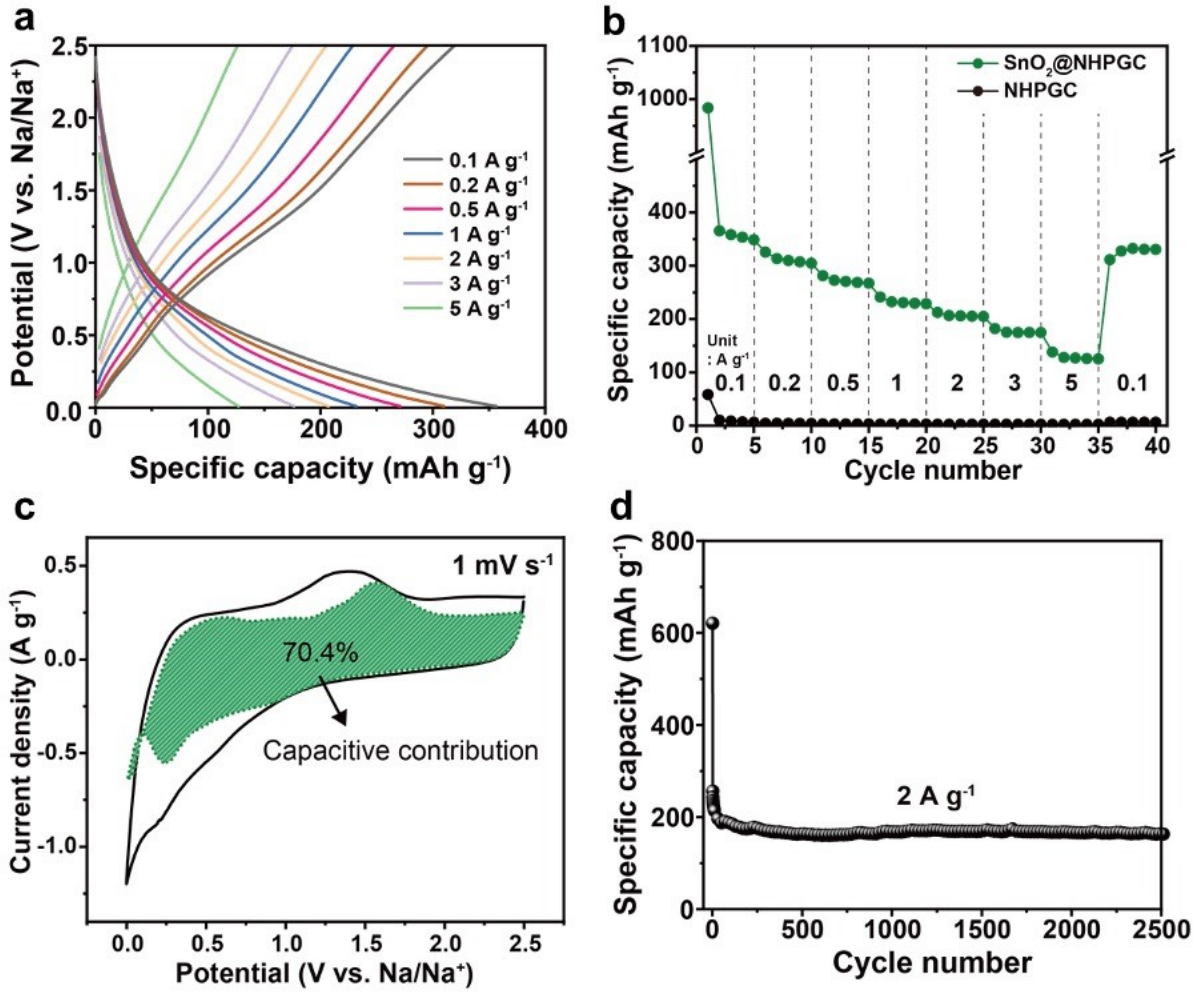

Figure S24. Electrochemical performances of SnO_2@NHPGC. (a) GCD curves, (b) rate performances, (c) capacitive contributions, and (d) cycling performance of SnO_2@NHPGC in 1 M $NaClO_4$ electrolyte for sodium storage.

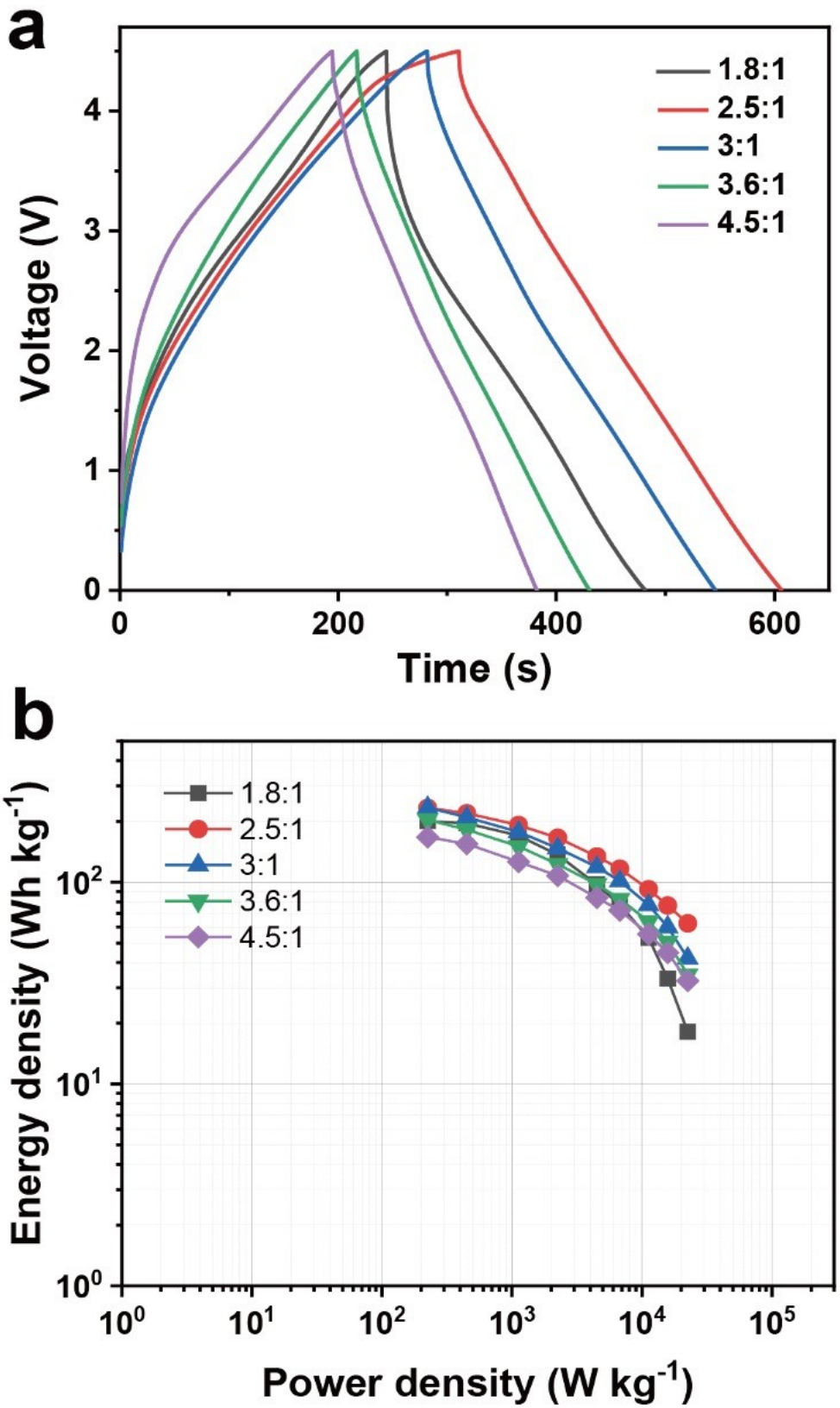

Figure S25. GCD and Ragone plot analyses. (a) GCD profiles at 1 A g^{-1} and (b) Ragone plot of NHPGC//SnO_2@NHPGC Li-ion HES cells in different cathode-to-anode mass ratios.

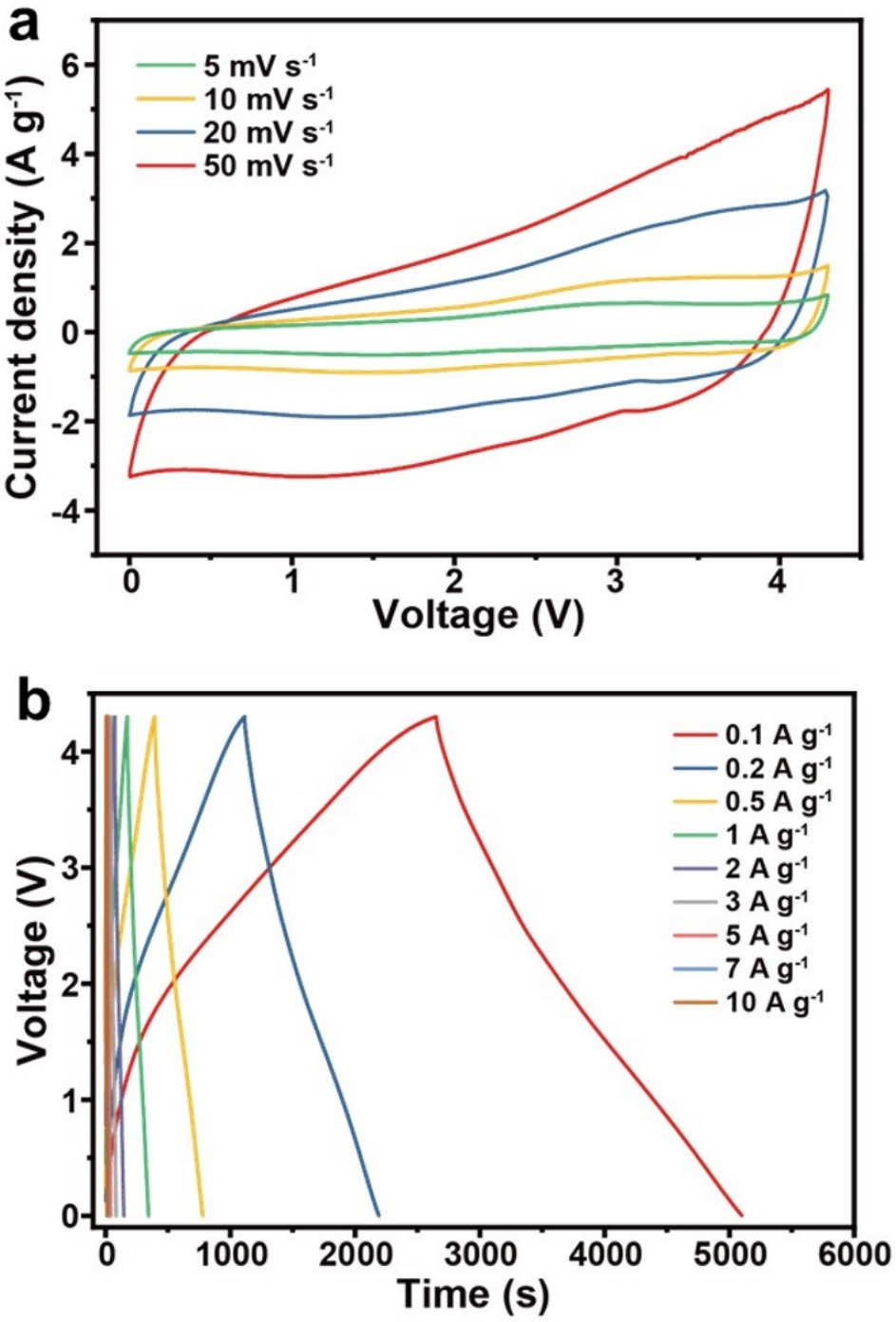

Figure S26. CV and GCD analyses. (a) CV and (b) GCD curves of NHPGC//SnO_2@NHPGC Na-ion HES in 1 M $NaClO_4$ electrolyte.

Table S1. Ratios of Co to Zn in Co_x-Zn_{10-x} MOF/GO measured by the ICP-OES analysis.

Sample	Zn-MOF /GO	Co_1-Zn_9 MOF/GO	Co_2-Zn_8 MOF/GO	Co_3-Zn_7 MOF/GO	Co-MOF /GO
Co/Zn	-	0.101	0.216	0.377	-

Table S2. Pore characteristics of Co_x-Zn_{10-x} NHPGC.

Sample	S_{BET} (m^2 g^{-1})	V_{pore} (cm^3 g^{-1})	V_{micro} (cm^3 g^{-1})	V_{meso} (cm^3 g^{-1})	V_{micro}/V_{meso} (%)
Zn-NHPGC	553	0.484	0.181	0.303	59.7
Co_1-Zn_9 NHPGC	554	0.641	0.161	0.480	33.5
Co_2-Zn_8 NHPGC	394	0.643	0.055	0.588	9.4
Co_3-Zn_7 NHPGC	278	0.459	0.037	0.422	8.8
Co-NHPGC	274	0.772	0.027	0.745	3.6

Table S3. Equivalent resistance (R_1) and electrolyte resistance (R_2) of Co_x-Zn_{10-x} NHPGC in Nyquist plot.

Sample	Zn-NHPGC	Co_1-Zn_9 NHPGC	Co-NHPGC
R_1	1.908 Ω	1.227 Ω	1.160 Ω
R_2	3.202 Ω	4.113 Ω	5.335 Ω

Table S4. Electrochemical performances of previously reported cathode materials and one by this work.

Cathode materials	Specific capacity	Voltage window (V)	BET surface area ($m^2\ g^{-1}$)	Surface area-normalized capacity ($\mu Ah\ m_{SSA}^{-2}$)	Ref.
3D hierarchical porous N-doped carbon (HNC)	62 mAh g^{-1} @ 0.2 A g^{-1}	3.0-4.5	992	62.50	2
B and N dual-doped carbon Nanofibers (BNC)	113 mAh g^{-1} @ 0.1 A g^{-1}	2.0–4.5	1076	105.02	3
Electrospun N-Doped hierarchical porous carbon nanofiber (a-PANF)	80 mAh g^{-1} @ 0.1 A g^{-1}	2.0-4.5	2157	37.09	4
3D porous activated nitrogen-doped graphene sheet (A-N-GS)	104 mAh g^{-1} @ 0.1 A g^{-1}	2.0-4.5	1083	96.03	5
nitrogen-doped carbon nanosheets (NCN)	62.7 mAh g^{-1} @ 0.2 A g^{-1}	3.0-4.5	1324	47.36	6
2D B/N co-doped carbon nanosheet (BCN)	90.5 mAh g^{-1} @ 0.1 A g^{-1}	2.0-4.5	601	150.58	7
Heteroatom-doped microporous carbon (MPC)	59.6 mAh g^{-1} @ 0.2 A g^{-1}	2.5-4.5	2675	22.28	8
NHPGC	123.4 mAh g^{-1} @ 0.1 A g^{-1}	2.0-4.5	553	223.15	This Work

Table S5. Electrochemical performances of Li-ion HES full cells by previous works and this work.

Cathode//Anode	Maximum Energy density (Power density)	Maximum power density (Energy density)	Voltage window (V)	Ref.
Li_3N/AC//SC	74.7 Wh kg^{-1} (75.1 W kg^{-1})	12900 W kg^{-1} (21.5 Wh kg^{-1})	2.0 - 4.0	9
AC//Zr-MOF	122.5 Wh kg^{-1} (250 W kg^{-1})	12500 W kg^{-1} (34.4 Wh kg^{-1})	1.0 - 4.0	10
AC//3S-Nb_2O_5-HoMSs	93.8 Wh kg^{-1} (112.5 W kg^{-1})	22500 W kg^{-1} (19.6 Wh kg^{-1})	1.0 - 3.5	11
G/AC//G/SC	151 Wh kg^{-1} (241 W kg^{-1})	18900 W kg^{-1} (83 Wh kg^{-1})	2.0 - 4.0	12
Spiral graphene //Hierarchically porous carbon	109 Wh kg^{-1} (1830 W kg_{-1})	5478 W kg^{-1} (91 Wh kg^{-1})	2.0 - 4.0	13
$CoSe_2$/SnSe//AC	131.03 Wh kg^{-1} (100 W kg_{-1})	12000 W kg^{-1} (38.33 Wh kg^{-1})	0.08 - 4.08	14
$LiMn_2O_4$ //Nitrogen-rich biomass carbon	50 Wh kg^{-1} (571 W kg^{-1})	6900 W kg^{-1} (17 Wh kg^{-1})	0 - 2.3 (aqueous)	15
NiCoP/NiCo-OH30 //Porous C	34 Wh kg^{-1} (775 W kg^{-1})	11600 W kg^{-1} (20 Wh kg^{-1})	0 - 1.6 (aqueous)	16
NHPGC//SnO_2@NHPGC	244.5 Wh kg^{-1} (225 W kg^{-1})	22500 W kg^{-1} (87.1 Wh kg^{-1})	0 - 4.5	This work

Table S6. Electrochemical performances of Na-ion HES full cells by previous works and this work.

Cathode//Anode	Maximum Energy density (Power density)	Maximum power density (Energy density)	Voltage window (V)	Ref.
NCN//$Fe_{1-x}S$	88 Wh kg^{-1} (150 W kg^{-1})	26 Wh kg^{-1} (11500 W kg^{-1})	0 - 3.0	17
STC-16//HAT-CNF-850	95 Wh kg^{-1} (190 W kg^{-1})	13000 W kg^{-1} (18 Wh kg^{-1})	0.5 - 4.0	18
AC//GCNF	55.58 W kg^{-1} (133 Wh kg^{-1})	4520 W kg^{-1} (18.19 Wh kg^{-1})	1.0 - 3.5	19
AC//FeS_2/TiO_2	73.7 Wh kg^{-1} (100 W kg^{-1})	10000 W kg^{-1} (20.6 Wh kg^{-1})	0 – 4.0	20
AC//graphite	60.5 Wh kg^{-1} (1422 W kg^{-1})	17127 W kg^{-1} (21.8 Wh kg^{-1})	0 – 3.9	21
AC//Fe_2S/rGO-NPC	110 Wh kg^{-1} (95 W kg^{-1})	20935 W kg^{-1} (74 Wh kg^{-1})	0.5 – 3.8	22
Nickel Hexacyanoferrate //Graphene	39.4 Wh kg^{-1} (333 W kg^{-1})	3333 W kg^{-1} (24.1 Wh kg^{-1})	0 – 2.0 (aqueous)	23
VC//Al_2O_3/C	30.8 Wh kg^{-1} (2016 W kg^{-1})	8064 W kg^{-1} (21 Wh kg^{-1})	0 – 2.0 (aqueous)	24
NHPGC//SnO_2@NHPGC	146.1 Wh kg^{-1} (215 W kg^{-1})	21500 W kg^{-1} (35.1 Wh kg^{-1})	0-4.3 V	This work

References

1 D. C. Marcano, D. V Kosynkin, J. M. Berlin, A. Sinitskii, Z. Sun, A. Slesarev, L. B. Alemany, W. Lu and J. M. Tour, *ACS Nano*, 2010, **4**, 4806–4814.

2 M. Yang, Y. Zhong, J. Ren, X. Zhou, J. Wei and Z. Zhou, *Adv. Energy Mater.*, 2015, **5**, 1500550.

3 Q. Xia, H. Yang, M. Wang, M. Yang, Q. Guo, L. Wan, H. Xia and Y. Yu, *Adv. Energy Mater.*, 2017, **7**, 1701336.

4 R. Shi, C. Han, X. Xu, X. Qin, L. Xu, H. Li, J. Li, C. P. Wong and B. Li, *Chem. - A Eur. J.*, 2018, **24**, 10460–10467.

5 R. Wang, Q. Zhao, W. Zheng, Z. Ren, X. Hu, J. Li, L. Lu, N. Hu, J. Molenda, X. Liu and C. Xu, *J. Mater. Chem. A*, 2019, **7**, 19909–19921.

6 S. Li, J. Chen, M. Cui, G. Cai, J. Wang, P. Cui, X. Gong and P. S. Lee, *Small*, 2017, **13**, 1602893.

7 Y. Hao, S. Wang, Y. Shao, Y. Wu and S. Miao, *Adv. Energy Mater.*, 2020, **10**, 1902836.

8 G. Zhu, T. Chen, L. Wang, L. Ma, Y. Hu, R. Chen, Y. Wang, C. Wang, W. Yan, Z. Tie, J. Liu and Z. Jin, *Energy Storage Mater.*, 2018, **14**, 246–252.

9 C. Sun, X. Zhang, C. Li, K. Wang, X. Sun and Y. Ma, *Energy Storage Mater.*, 2020, **24**, 160–166.

10 W. Yan, J. Su, Z. M. Yang, S. Lv, Z. Jin and J. L. Zuo, *Small*, 2021, **17**, 2005209.

11 R. Bi, N. Xu, H. Ren, N. Yang, Y. Sun, A. Cao, R. Yu and D. Wang, *Angew. Chemie*, 2020, **132**, 4895–4898.

12 Y. An, T. Liu, C. Li, X. Zhang, T. Hu, X. Sun, K. Wang, C. Wang and Y. Ma, *J. Mater. Chem. A*, 2021, **9**, 15654–15664.

13 G. Li, Z. Yin, H. Guo, Z. Wang, G. Yan, Z. Yang, Y. Liu, X. Ji and J. Wang, *Adv. Energy Mater.*, 2019, **9**, 1802878.

14 S. Tao, R. Momen, Z. Luo, Y. Zhu, X. Xiao, Z. Cao, D. Xiong, W. Deng, Y. Liu, H. Hou, G. Zou and X. Ji, *Small*, 2023, **19**, 2207975.

15 C. Li, W. Wu, S. Zhang, L. He, Y. Zhu, J. Wang, L. Fu, Y. Chen, Y. Wu and W. Huang, *J. Mater. Chem. A*, 2019, **7**, 4110–4118.

16 X. Li, H. Wu, A. M. Elshahawy, L. Wang, S. J. Pennycook, C. Guan and J. Wang, *Adv. Funct. Mater.*, 2018, **28**, 1800036.

17 S. Li, J. Chen, X. Gong, J. Wang and P. S. Lee, *Small*, 2018, **14**, 1804035.

18 R. Yan, E. Josef, H. Huang, K. Leus, M. Niederberger, J. P. Hofmann, R. Walczak, M. Antonietti and M. Oschatz, *Adv. Funct. Mater.* **2019**, *29*, 1902858.

19 M. L. Divya, S. Jayaraman, Y. S. Lee and V. Aravindan, *Chem. Eng. J.*, 2021, **426**, 130892.

20 X. Xiao, X. Duan, Z. Song, X. Deng, W. Deng, H. Hou, R. Zheng, G. Zou and X. Ji, *Adv. Funct. Mater.*, 2022, **32**, 2110476.

21 X. Liu, G. A. Elia, B. Qin, H. Zhang, P. Ruschhaupt, S. Fang, A. Varzi and S. Passerini, *ACS Energy Lett.*, 2019, **4**, 2675–2682.

22 Y. Song, X. Sun, L. Li, C. Zhang and F. Yin, *Carbon N. Y.*, 2023, **204**, 219–230.

23 K. Krishnamoorthy, P. Pazhamalai, S. Sahoo, J. H. Lim, K. H. Choi and S. J. Kim, *ChemElectroChem*, 2017, **4**, 3302–3308.

24 E. B. T, H. Tanaya Das, T. Maiyalagan and N. Das, *J. Alloys Compd.*, 2023, **931**, 167501.